J. Fluid Mech. (1996), vol. 318, pp. 303–337

Linear processes in unsteady stably stratified turbulence

By H. HANAZAKI[1]† AND J. C. R. HUNT[1,2]

[1] Department of Applied Mathematics and Theoretical Physics, University of Cambridge, Silver Street, Cambridge, CB3 9EW, UK

[2] Meteorological Office, London Road, Bracknell, Berkshire, RG12 2SZ, UK

(Received 28 July 1995)

Unsteady turbulence in uniformly stratified unsheared flow is analysed using rapid distortion theory (RDT). For inviscid flow with no molecular diffusion the theory shows how the initial conditions, such as the initial turbulent kinetic energy KE_0 and potential energy PE_0, determine the partition of energy between the potential energy associated with density fluctuation and the kinetic energy associated with each of the velocity components during the subsequent development of the turbulence. One parameter is an exception to this sensitivity to initial conditions, namely the limit at large time of the ratio of potential energy to vertical kinetic energy. In the linear theory, this ratio depends neither on the Reynolds number Re, nor the Prandtl number Pr nor the Froude number Fr. This is consistent with turbulence measurements in the atmosphere, wind tunnel and water tank experiments, and with large-eddy simulations, where similar values of the ratio are found. The RDT results are extended to show the effects of viscosity and diffusion where Re is not very large, explaining the sensitivity of the spectra and the fluxes to the value of the Prandtl number Pr. When Pr is larger than 1, the high-wavenumber components of the three-dimensional spectra induce a vertical flux of temperature (density) that is positive (negative), and therefore 'countergradient.' On the other hand, when the thermal diffusivity is stronger and Pr is less than 1, lower-wavenumber components become countergradient sooner since the high-wavenumber components are prevented from becoming countergradient. When all the wavenumber components are integrated to derive the total vertical density flux, it becomes countergradient more quickly and more strongly in high-Pr than in low-Pr turbulence. All these theoretically derived differences between high-Pr and low-Pr turbulence are consistent with the experimental measurements in water tank and wind tunnel experiments and numerical simulations. It is shown that the initial kinetic and potential energy spectrum forms $E(k)$ and $S(k)$ near $k = 0$ determine the long-time limit values of the variances and the covariances, including their decay rate with time. In the special case of $Pr = 1$, the oscillation time period of the three-dimensional spectrum function is independent of the wavenumber and is the same as that of an inviscid fluid with the effect of viscosity/diffusion being limited to the damping of all the wavenumber components in-phase with each other. Furthermore, the non-dimensional ratios of the covariances, including the normalized vertical density flux and the anisotropy tensor, agree with the inviscid results if $S(k)$ is proportional to $E(k)$, or if either $S(k)$ or $E(k)$ is identically zero. However, even when $Pr = 1$, in the 'one-dimensional spectrum' in the x-direction, there is a transitory countergradient flux for high wavenumbers; only in this case is there a qualitative difference with the three-dimensioanl spectrum. This

† Present address: National Institute for Environmental Studies, Tsukuba, Ibaraki 305, Japan.

paper shows that the characteristic differences in the behaviour of stably stratified turbulence reported in previous DNS experiments at moderate Reynolds numbers can largely be explained by linear oscillations and simple molecular or eddy diffusion rather than by any new kinds of nonlinear mixing processes.

1. Introduction

The transport of mass and heat in the atmosphere and ocean depends critically on how turbulence is affected by the presence of the stable density gradients in these flows. Recent laboratory experiments and numerical simulations on the unsteady turbulence in uniformly stratified fluid have shown how these effects are quite complex even without mean shear. Since the effects of stratification obviously affect the vertical transfer of both the dynamical scalars, heat or density, and the passive scalars, e.g. the concentrations of a pollutant, the most controversial and unresolved problem has been the qualitative and quantitative explanation of the countergradient transport of dynamical and passive scalars, which means that the heat and mass are transported by turbulent flux against the stratification. The phenomenon is sometimes observed as a net time-averaged effect (e.g. Komori *et al.* 1983) but often only as a weak transient effect (e.g. Itsweire, Helland & Van Atta, 1983; Lienhard & Van Atta 1990; Yoon & Warhaft 1990). Similar effects have been noted in several numerical simulations such as that of Gerz & Yamazaki (1993). With little theoretical justification, this mechanism has hitherto been explained by the nonlinear, oscillatory turbulent 'mixing' of fluid. However, any theoretical explanations should clarify in which respect the phenomenon is nonlinear, and in which respect it is linear; a fuller knowledge of the linear effect should be the starting point of the study of nonlinear phenomena.

In this theoretical study we examine linear mechanisms for stratification effects and in particular for the countergradient flux. We apply linear rapid distortion theory (RDT) to unsheared stratified turbulence and obtained the analytical form of the three-dimensional spectrum functions, with the aim of understanding the differences in the time-dependent spectral behaviour of the low ($Pr < 1$) and high ($Pr > 1$) Prandtl number flows. We also show the special character of turbulence when $Pr = 1$, which surprisingly is in many respects similar to that of a non-diffusive fluid. Deissler (1962) first used this approach, by calculating linearized two-point correlation equations to show the difference of the form of three-dimensional spectrum functions when the Prandtl number is 0.7 and 10. Our calculations are more general in that the effects of the initial conditions, in particular the effect of the initial turbulent kinetic/potential energy and their spectral form, are considered. These calculations extend those of Hunt, Stretch & Britter (1988), by obtaining the results in analytical form so that several new insights emerge. We note that the dependence on Pr is different in one-dimensional spectra and three-dimensional spectra near $Pr = 1$. This difference is important since in experiments only the one-dimensional spectra are measured. We also consider those long-time asymptotics of the covariances that change with time very slowly or not at all, because, as explained by Townsend (1976) and Hunt & Carruthers (1990), these particular asymptotic results of linear theories are often applicable to steady-state turbulent flows, such as those in atmospheric and oceanic stratified turbulence. We have compared our theoretical results with recent experiments and direct numerical simulations (DNS). The comparison of our theory

with the experiments and DNS helps clarify which are the truly linear and nonlinear phenomena in these flows.

2. RDT equations

We consider a homogeneous unsheared turbulent flow placed in a uniform density gradient $(\mathrm{d}\overline{\rho}/\mathrm{d}x_3)$ in the x_3-direction, which is anti-parallel to the gravitational acceleration. The governing equations by rapid distortion theory (RDT) (Townsend 1976) in the frame of reference moving with the uniform mean flow are

$$\left(\frac{\mathrm{d}}{\mathrm{d}t} + \nu k^2\right)\hat{u}_i = \left(\frac{k_i k_3}{k^2} - \delta_{i3}\right)\hat{\rho}, \tag{2.1}$$

$$\left(\frac{\mathrm{d}}{\mathrm{d}t} + \kappa k^2\right)\hat{\rho} = N^2\hat{u}_3, \tag{2.2}$$

where N is the Brunt–Väisälä frequency given by $N^2 = -(g/\rho_0)(\mathrm{d}\overline{\rho}/\mathrm{d}x_3)$, and the Fourier coefficients $\hat{u}_i (i = 1, 2, 3)$ and $\hat{\rho}$ are defined in terms of the velocity and density fluctuation by

$$u_i = \sum_{\boldsymbol{k}} \hat{u}_i(\boldsymbol{k}, t)\mathrm{e}^{\mathrm{i}\boldsymbol{k}\cdot\boldsymbol{x}}, \tag{2.3}$$

and

$$\frac{g}{\rho_0}\rho = \sum_{\boldsymbol{k}} \hat{\rho}(\boldsymbol{k}, t)\mathrm{e}^{\mathrm{i}\boldsymbol{k}\cdot\boldsymbol{x}}. \tag{2.4}$$

Here, ρ_0 is the reference density, ρ is the perturbation density, ν is the viscosity coefficient and κ is the diffusion coefficient. When there is no shear, the wavenumber does not change with time and

$$\frac{\mathrm{d}k_i}{\mathrm{d}t} = 0, \tag{2.5}$$

which greatly simplifies the subsequent analysis. Note that in (2.1), the pressure gradient is replaced by an exact expression in terms of $\hat{\rho}$.

In the non-dimensionalized form of the governing equations (2.1), (2.2), there are three non-dimensional parameters, i.e. the Prandtl number $Pr = \nu/\kappa$, the Reynolds number of the turbulence $Re = UL/\nu$, and the Froude number $Fr = U/NL$ (e.g. Riley, Metcalfe & Weissman 1981). While the Prandtl number is a constant of the fluid, Re and Fr are defined by the local turbulence parameters L, the integral length scale and U the r.m.s. velocity, which is determined by the large-scale eddies. The relative effects of viscous stresses and stable stratification on different sizes (l) of the eddies, whose velocities are $u(l)$, are characterized by 'eddy' Reynolds and Froude numbers defined as $Re_l = u(l)l/\nu$ and $Fr_l = u(l)/Nl$.

However, for characterizing the overall features of laboratory experiments where the length scale and r.m.s. turbulence velocity vary with time (in the moving frame), it is conventional to use the 'mean flow' Froude number $\overline{Fr} = \overline{U}/NL_0$ and the mean flow Reynolds number $\overline{Re} = \overline{U}L_0/\nu$, where $\overline{U}$ is the mean velocity and L_0 is the grid size often denoted by M. Since in most experiments $U \sim 10^{-2}\overline{U}$, it follows that $\overline{Fr} \gg Fr$.

It is important to note the conditions for which the RDT in stably stratified flow is valid. They are given by the conditions that the nonlinear term $(\boldsymbol{u}\cdot\nabla)\boldsymbol{u}$ ($\boldsymbol{u} = (u_1, u_2, u_3)$, $|\boldsymbol{u}| = O(u)$) in the Navier–Stokes equations is small compared to the buoyancy term $g\rho/\rho_0$ (Derbyshire & Hunt 1985), and that the term $(\boldsymbol{u}\cdot\nabla)\rho$ is small compared to

$u_3 \mathrm{d}\bar{\rho}/\mathrm{d}x_3$. Using the eddy size l and its characteristic velocity $u(l)$, the nonlinear term in (2.1) is expressed as†

$$(\boldsymbol{u}\cdot\nabla)\boldsymbol{u} = O\left(\frac{u^2}{l}\right), \tag{2.6}$$

while the buoyancy term is

$$\begin{aligned}\frac{g}{\rho_0}\rho &= O(uN^2t) \quad \text{if } Nt \ll 1\\ &= O(uN) \quad \text{if } Nt \geqslant 1 \text{ and } Fr_l = \frac{u}{Nl} \ll 1,\end{aligned}$$

where Fr_l is the eddy Froude number, and the buoyancy advection term is

$$\begin{aligned}(\boldsymbol{u}\cdot\nabla)\rho &= O\left(uNt\frac{\mathrm{d}\bar{\rho}}{\mathrm{d}x_3}\right)\\ &= O\left(u\frac{u}{Nl}\frac{\mathrm{d}\bar{\rho}}{\mathrm{d}x_3}\right),\end{aligned} \tag{2.7}$$

for these two conditions. Once t is greater than the oscillation period N^{-1}, Fr_l is a measure of nonlinearity, and therefore the RDT approximations, i.e. (2.1) and (2.2) are valid if $Fr_l \ll 1$.

Since

$$\frac{u}{l} = O\left(\frac{U}{L}\right) \text{ (at low and moderate } Re\text{)}, \tag{2.8a}$$

$$= O\left(\epsilon^{1/3}l^{-2/3}\right)$$

(at high Re, where ϵ is the local turbulence energy dissipation rate), (2.8b)

the condition $Fr_l \ll 1$ can be related to a condition applying to the Froude number for the energy-containing eddies $Fr(= U/NL)$. At low and moderate Re,

$$Fr_l \ll 1 \implies Fr \ll 1, \tag{2.9a}$$

and at high Re,

$$Fr_l \ll 1 \implies \frac{\epsilon^{1/3}}{Nl^{2/3}} \ll 1, \text{ or } Fr\left(\frac{L}{l}\right)^{2/3} \ll 1. \tag{2.9b}$$

Thus in laboratory experiments and DNS for low- or moderate-Re flows, RDT is valid for low values of Fr. On the other hand, it is clear from (2.9b) that at high Re, for the smaller scales of turbulence with $l/L < Fr^{3/2}$, Fr_l satisfies $Fr_l \geqslant 1$ so that RDT is not valid for all scales of motion even if Fr is small. This is consistent with the well established experimental results of geophysical turbulence where it is found that at small scales the turbulence is not affected by body forces (see for example the review by Hunt & Vassilicos 1991).

We consider in this paper only the unbounded fluid and do not consider the effect of the outer solid boundary that usually exists in laboratory experiments. The effect of the periodic boundary condition, usually used in DNS, has also to be considered for a more complete comparison with the numerical simulations. These effects could be considered using the methods described in this paper.

† Note also that the nonlinear terms neglected in (2.1) and (2.2) are the Fourier coefficients of the eddy inertial term $(\boldsymbol{u}\cdot\nabla)\boldsymbol{u}$ and of the eddy density-gradient acceleration term $(\boldsymbol{u}\cdot\nabla)\rho$.

3. Inviscid fluid

3.1. *Calculation for spectra*

We first consider the inviscid fluid. In this case the analytical results confirm and extend the previous numerical solutions of the inviscid RDT equations by Hunt *et al.* (1988). The results also explain the short-time development obtained in experiments and DNS where the effect of viscosity and diffusion are negligible. By assuming $\nu = \kappa = 0$ in (2.1)–(2.5) we obtain $\hat{u}_i$ $(i = 1, 2, 3)$ and $\hat{\rho}$ as

$$\hat{\rho} = \hat{\rho}_0 \cos at + \frac{N^2}{a}\hat{u}_{30} \sin at, \tag{3.1}$$

$$\hat{u}_1 = \hat{u}_{10} + \frac{k_1 k_3}{k^2}\left[\frac{\hat{\rho}_0}{a}\sin at - \frac{N^2}{a^2}\hat{u}_{30}(\cos at - 1)\right], \tag{3.2}$$

$$\hat{u}_2 = \hat{u}_{20} + \frac{k_2 k_3}{k^2}\left[\frac{\hat{\rho}_0}{a}\sin at - \frac{N^2}{a^2}\hat{u}_{30}(\cos at - 1)\right], \tag{3.3}$$

$$\hat{u}_3 = \frac{1}{N^2}\frac{\mathrm{d}\hat{\rho}}{\mathrm{d}t} = \hat{u}_{30}\cos at - \frac{a}{N^2}\hat{\rho}_0 \sin at, \tag{3.4}$$

where

$$a = \frac{(k_1^2 + k_2^2)^{1/2}}{k}N, \tag{3.5}$$

and the subscript 0 denotes the initial values.

Then we can calculate all the three-dimensional spectrum functions. The results are

$$\begin{aligned}\Phi_{\rho 3}(\boldsymbol{k}, t) &= \tfrac{1}{2}\overline{\hat{\rho}^* \hat{u}_3 + \hat{\rho}\hat{u}_3^*} \\ &= \left[-\frac{a}{2N^2}\Phi_{\rho\rho}(\boldsymbol{k}, 0) + \frac{N^2}{2a}\Phi_{33}(\boldsymbol{k}, 0)\right]\sin 2at,\end{aligned} \tag{3.6}$$

$$\begin{aligned}\Phi_{11}(\boldsymbol{k}, t) = \Phi_{11}(\boldsymbol{k}, 0) &+ \frac{k_1^2 k_3^2}{k^4}\left[\frac{1}{a^2}\Phi_{\rho\rho}(\boldsymbol{k}, 0)\sin^2 at + \frac{N^4}{a^4}\Phi_{33}(\boldsymbol{k}, 0)(\cos at - 1)^2\right] \\ &- \frac{k_1 k_3}{k^2}\frac{2N^2}{a^2}\Phi_{13}(\boldsymbol{k}, 0)(\cos at - 1),\end{aligned} \tag{3.7}$$

$$\begin{aligned}\Phi_{33}(\boldsymbol{k}, t) = \Phi_{33}(\boldsymbol{k}, 0) &- 2\frac{k_1^2 + k_2^2}{k^2}\left[\frac{1}{4N^2}\Phi_{\rho\rho}(\boldsymbol{k}, 0)(\cos 2at - 1)\right. \\ &\left. - \frac{N^2}{4a^2}\Phi_{33}(\boldsymbol{k}, 0)(\cos 2at - 1)\right],\end{aligned} \tag{3.8}$$

$$\Phi_{\rho\rho}(\boldsymbol{k}, t) = \Phi_{\rho\rho}(\boldsymbol{k}, 0) + 2N^2\left[\frac{1}{4N^2}\Phi_{\rho\rho}(\boldsymbol{k}, 0)(\cos 2at - 1) - \frac{N^2}{4a^2}\Phi_{33}(\boldsymbol{k}, 0)(\cos 2at - 1)\right], \tag{3.9}$$

where an overbar denotes the ensemble average.

In this study we assume the initial density fluxes to be zero, i.e.

$$\Phi_{\rho i}(\boldsymbol{k}, 0) = 0 \ (i = 1, 2, 3), \tag{3.10}$$

as in the previous numerical simulations. Although some laboratory experiments (e.g. Lienhard & Van Atta 1990) suggest $\overline{\rho u_3}(t = 0) \neq 0$, we ignore this possibility because there is no information about the initial spectral form of $\Phi_{\rho 3}(\boldsymbol{k}, 0)$. Therefore, throughout this study, theoretical (RDT) results are confined to the case of

$\Phi_{\rho i}(\boldsymbol{k},0) = 0$ $(i = 1,2,3)$. The effects of non-zero $\Phi_{\rho i}(\boldsymbol{k},0)$ could be assessed by exactly following the method described hereafter.

If in addition we assume that the initial velocity and density perturbations are both isotropic, the initial conditions are given by

$$\Phi_{ij}(\boldsymbol{k},0) = \frac{E(k)}{4\pi k^2}\left(\delta_{ij} - \frac{k_i k_j}{k^2}\right), \tag{3.11}$$

and

$$\Phi_{\rho\rho}(\boldsymbol{k},0) = \frac{S(k)}{4\pi k^2} 2N^2. \tag{3.12}$$

Here

$$KE_0 = \int_0^\infty E(k)\mathrm{d}k, \tag{3.13}$$

and

$$PE_0 = \frac{1}{2N^2}\int \Phi_{\rho\rho}(\boldsymbol{k},0)\mathrm{d}\boldsymbol{k} = \int_0^\infty S(k)\mathrm{d}k, \tag{3.14}$$

are the initial turbulent kinetic and potential energy.

We now write the wavenumber vector in spherical coordinates as

$$k_1 = k\sin\theta\cos\phi, \quad k_2 = k\sin\theta\sin\phi, \quad k_3 = k\cos\theta, \tag{3.15}$$

so that

$$k^2 = k_1^2 + k_2^2 + k_3^2, \tag{3.16}$$

and

$$\sin\theta = \frac{(k_1^2 + k_2^2)^{1/2}}{k} = \frac{k_H}{k}, \tag{3.17}$$

where the horizontal wavenumber k_H is defined by

$$k_H = (k_1^2 + k_2^2)^{1/2}. \tag{3.18}$$

3.2. *Variances and covariances*

Substituting (3.11) and (3.12) into (3.6), we obtain the vertical flux of density as

$$\begin{aligned}\overline{\rho u_3}(t) &= \int \Phi_{\rho 3}(\boldsymbol{k},t) 2\pi k^2 \mathrm{d}k \sin\theta \mathrm{d}\theta \\ &= \frac{N}{4} E_0^{(C)} \int_0^\pi \mathrm{d}\theta \sin^2\theta \sin(2Nt\sin\theta),\end{aligned} \tag{3.19}$$

where $E_0^{(C)} = KE_0 - 2PE_0$ is the complementary energy.

Other variances and covariances can be calculated similarly and the results are:

$$\overline{u_1^2}(t) = \overline{u_2^2}(t) = \tfrac{7}{12}KE_0 + \tfrac{1}{6}PE_0 + \tfrac{1}{8}E_0^{(C)}\int_0^\pi \mathrm{d}\theta \cos^2\theta \sin\theta \cos(2Nt\sin\theta), \tag{3.20}$$

$$\overline{u_3^2}(t) = \tfrac{1}{3}(KE_0 + 2PE_0) + \tfrac{1}{4}E_0^{(C)}\int_0^\pi \mathrm{d}\theta \sin^3\theta \cos(2Nt\sin\theta), \tag{3.21}$$

and

$$\overline{\rho^2}(t) = \tfrac{1}{2}N^2(KE_0 + 2PE_0) - \tfrac{1}{4}N^2 E_0^{(C)}\int_0^\pi \mathrm{d}\theta \sin\theta \cos(2Nt\sin\theta). \tag{3.22}$$

Some examples are plotted in figure 1 for two initial conditions PE_0/KE_0=0 and $\frac{1}{3}$.

The latter is the case when the potential energy is equal to the vertical kinetic energy (cf. figure 3 of Hunt *et al.* 1988). Note here that, as for inviscid unstratified shear flow (Townsend 1976), all these functions depend only on the total initial kinetic and potential turbulence energy (KE_0 and PE_0) and not on the precise form of the initial kinetic and potential energy spectra $E(k)$ or $S(k)$. We also note that, as expected for a linear analysis, the oscillation periods of these functions are completely independent of the initial conditions and depend only on the value of N. Accordingly the zeros of $\overline{\rho u_3}(t)$ are determined only by an integral that contains Nt. On the other hand, the oscillation amplitudes are determined by $E_0^{(C)}$. Then, the unsteady part of the covariances all vanish when $E_0^{(C)} = 0$. This corresponds to the initial equilibrium state of the turbulence. When $PE_0 = 0$, the value of $E_0^{(C)}$ is KE_0, while when $PE_0 = \frac{1}{3}KE_0$, it is $\frac{1}{3}KE_0$, which leads to an amplitude that is only $\frac{1}{3}$ as large (see figure 1*d*).

The short and long time limit of variances in (3.19)–(3.22) are as follows. When $Nt \ll 1$,

$$\overline{\rho u_3}(t) = \tfrac{2}{3}N^2 t E_0^{(C)}, \tag{3.23a}$$

$$\overline{u_1^2}(t) = \overline{u_2^2}(t) = \tfrac{2}{3}KE_0 - \tfrac{1}{15}E_0^{(C)}N^2t^2, \tag{3.23b}$$

$$\overline{u_3^2}(t) = \tfrac{2}{3}KE_0 - \tfrac{8}{15}E_0^{(C)}N^2t^2, \tag{3.23c}$$

$$\overline{\rho^2}(t) = 2N^2PE_0 + \tfrac{2}{3}E_0^{(C)}N^4t^2. \tag{3.23d}$$

Using these results, we can calculate $\overline{\rho u_3}/(\overline{\rho^2}^{1/2}\overline{u_3^2}^{1/2})$ in the limit of $t \to 0$. If we substitute $KE_0 = 0$, we obtain $\overline{\rho u_3}/(\overline{\rho^2}^{1/2}\overline{u_3^2}^{1/2})(t \to 0) = -(5/6)^{1/2} = -0.913$. This agrees with the published DNS result of Gerz & Yamazaki (1993), which show $\overline{\rho u_3}/(\overline{\rho^2}^{1/2}\overline{u_3^2}^{1/2})(t \to 0) = -0.914$ (Dr Gerz has privately communicated that the value was actually −0.913). The value obtained by a separate linear theory of Chasnov considering only the limit of $t \to 0$ (see the Appendix in Gerz & Yamazaki) is $-(5/6)^{1/2}$ and exactly agrees with our results. (Note that the sign of the vertical density flux changes when we use the temperature instead of the density. In RDT, the effect of pressure is incorporated implicitly.) If we substitute $PE_0 = 0$ into (3.23), we obtain $\overline{\rho u_3}/(\overline{\rho^2}^{1/2}\overline{u_3^2}^{1/2})(t \to 0) = 1$. If we substitute $KE_0 = \frac{3}{2}\overline{u_3^2}(0)$ and $PE_0 = 0$, we recover the short-time approximation of Hunt *et al.* (1988) (see their §2.3.1).

The long-time ($Nt \gg 1$) approximations are obtained from (3.19)–(3.22) using the method of steepest descents as

$$\overline{\rho u_3}(t) = \tfrac{1}{4}NE_0^{(C)}\left(\frac{\pi}{Nt}\right)^{1/2}\sin\left(2Nt - \tfrac{1}{4}\pi\right), \tag{3.24a}$$

$$\overline{u_1^2}(t) = \overline{u_2^2}(t) = \tfrac{7}{12}KE_0 + \tfrac{1}{6}PE_0, \tag{3.24b}$$

$$\overline{u_3^2}(t) = \tfrac{1}{3}(KE_0 + 2PE_0) + \tfrac{1}{4}E_0^{(C)}\left(\frac{\pi}{Nt}\right)^{1/2}\cos\left(2Nt - \tfrac{1}{4}\pi\right), \tag{3.24c}$$

$$\overline{\rho^2}(t) = \tfrac{1}{2}N^2(KE_0 + 2PE_0) - \tfrac{1}{4}N^2E_0^{(C)}\left(\frac{\pi}{Nt}\right)^{1/2}\cos\left(2Nt - \tfrac{1}{4}\pi\right). \tag{3.24d}$$

This analytical method shows that the time-dependent part of (3.24) comes from near $k_3 = 0\,(\theta = \pi/2)$, which means infinite vertical wavelength. This suggests that, when we consider the long-time development, we have to consider the effect of the 'finite' extent of fluid that we usually encounter in laboratory experiments. Exact comparison with DNS requires consideration of the periodic boundary conditions. However, the effects are important only in the unsteady part of (3.19)–(3.22). Then,

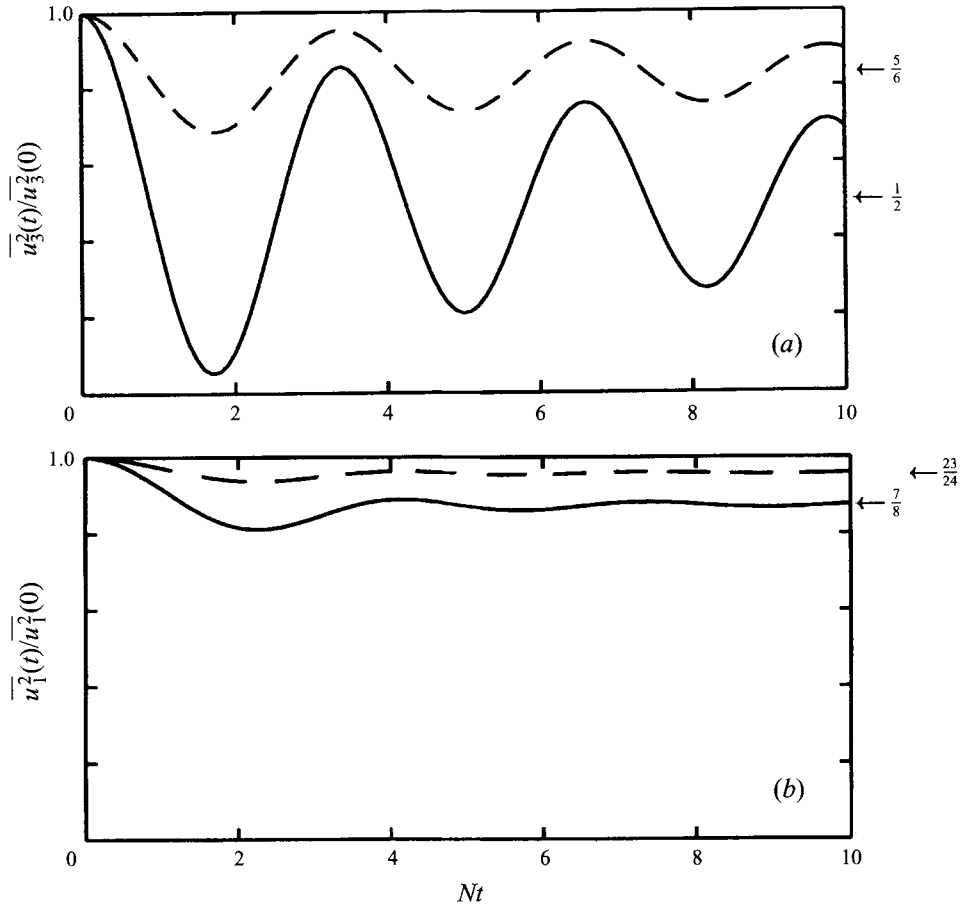

FIGURE 1 (*a*, *b*). For caption see facing page.

while the unsteady part decays with time, the steady part becomes dominant at long time and therefore the confinement effect is not actually significant.

It is important to note that the oscillating parts of the variances and the covariances decay with time in proportion to $t^{-1/2}$ even without viscosity and nonlinearity. The damping of oscillation is essentially a characteristic of inviscid fluid without nonlinearity. The expressions (3.6)–(3.9) for the three-dimensional spectra show that the oscillation period T is given by $T = \pi/a = \pi k/(Nk_H)$. This means that if we look at the time variation on the time scale of $Nt/\pi \approx 1$ as is usually done, the spectral components which satisfy $k/k_H = \sin^{-1}\theta \approx 1$, i.e. $\theta \approx \pi/2$, are distorted significantly, while the distortion is very small in the spectral region where $k/k_H \gg 1$, i.e. where $\theta \approx 0, \pi$. This is the reason why in the unsteady part of the variances and the covariances, the contribution from a certain part of the wavenumber space $k_H/k \approx 1$ ($\theta \approx \pi/2$) is dominant and the contributions from other components are less effective. As time proceeds ($Nt \gg 1$) the contributing region of θ becomes much more restricted to a narrower band near $\theta = \pi/2$ and the value of the integral decays with time.

We also note that the oscillation period asymptotes in a long time to $t = \pi/N$, which is the period of buoyancy oscillation. It is noteworthy that in the long-

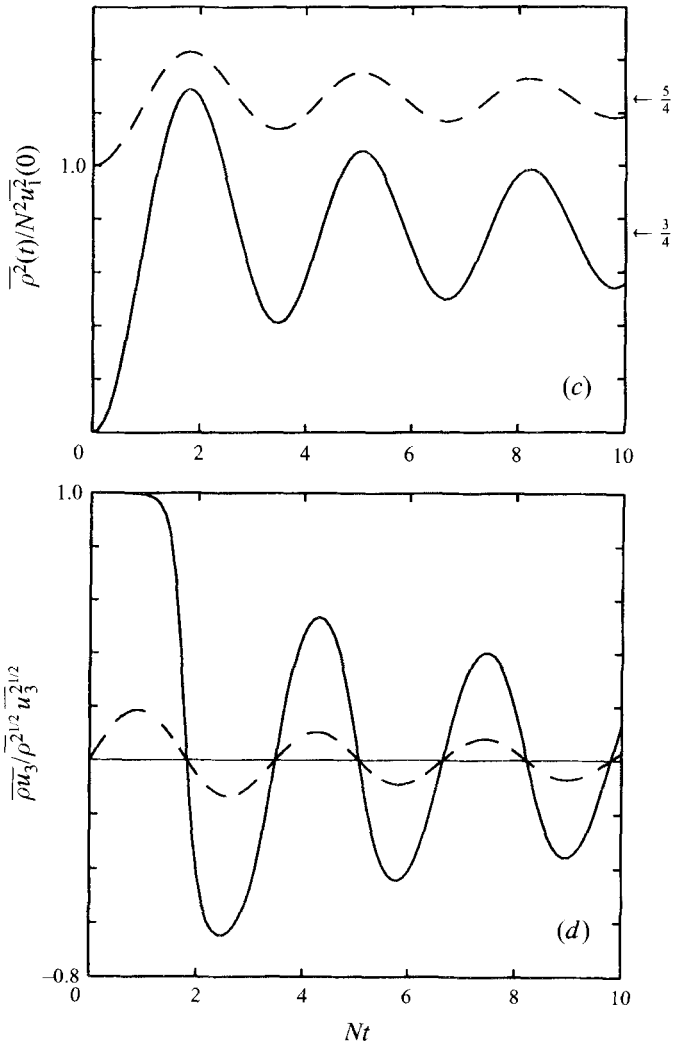

FIGURE 1. Time development of the covariances in inviscid fluid using RDT. Solid lines show the results for $PE_0 = 0$ and the dashed lines show the results for $PE_0 = \frac{1}{3}KE_0$. The arrows show the values in the long-time limit. (*a*) $\overline{u_3^2}(t)/\overline{u_3^2}(0)$; (*b*) $\overline{u_1^2}(t)/\overline{u_1^2}(0)$; (*c*) $\overline{\rho^2}(t)/N^2\overline{u_1^2}(0)$; (*d*) $\overline{\rho u_3}/(\overline{\rho^2}^{1/2}\overline{u_3^2}^{1/2})(t)$.

time approximation of $\overline{u_1^2}(t)$, the time-dependent term vanishes. This shows that the fluctuation in the horizontal kinetic energy decays rapidly, faster than $\propto t^{-1/2}$.

It is of interest to note that the energy ratio ER of potential energy to vertical kinetic energy, $ER \equiv (\overline{\rho^2}/2N^2)/(\overline{u_3^2}/2)$, is equal to 3/2 in the long-time limit, independent of the initial conditions KE_0 and PE_0, provided the initial turbulence is isotropic. This asymptotic value is also the same in the viscous/diffusive fluid irrespective of the Prandtl number, Reynolds number and the initial conditions (see §4). The value roughly agrees with the observed value of about $ER = 1.0 \pm 0.3$ in the atmosphere (Nieuwstadt 1984; Hunt, Kaimal & Gaynor 1985). Wind tunnel experiments ($Pr = 0.7$) by Yoon & Warhaft (1990, their figure 20) show that the value ER is less than 1, but the largest time ($Nt \approx 3$) attained is not large enough for comparison with the long-time-limit theoretical value. The experiments for two-layer thermally stratified

fluid ($Pr = 6$) by Komori & Nagata (1995) show that, for the largest time ($Nt = 5.6$) attained, the ratio ER is about 1.25, although there is still some tendency for it to increase with time. For the case of salt water ($Pr \sim 600$), LES for shear flow gives a value of $ER \approx 2.3$ for Richardson number $Ri = 1.0$, but this tends to reduce for larger Richardson numbers (see figure 8 of Schumann & Gerz 1995). Under the limit of no diffusion($\kappa \to 0$) and $Nt \to \infty$, Pearson, Puttock & Hunt (1983) showed that the energy ratio approaches $ER \simeq \frac{1}{2}\overline{\zeta^2}$, where $\overline{\zeta^2}$ is a coefficient of $O(1)$ depending on the spectrum of turbulence, which decreases with Fr and its maximum is less than 2.

3.3. *Special cases*

When $PE_0 = 0$ (and $KE_0 = \frac{3}{2}\overline{u_1^2}(0) = \frac{3}{2}\overline{u_3^2}(0)$), we obtain the steady part of (3.24) (or in the limit of $Nt \to \infty$) as

$$\overline{\rho u_3}(\infty) = 0, \quad \overline{u_1^2}(\infty) = \overline{u_2^2}(\infty) = \tfrac{7}{8}\overline{u_1^2}(0), \quad \overline{u_3^2}(\infty) = \tfrac{1}{2}\overline{u_1^2}(0), \quad \overline{\rho^2}(\infty) = \tfrac{3}{4}N^2\overline{u_1^2}(0). \tag{3.25}$$

On the other hand, when $PE_0 = \frac{1}{3}KE_0 = \frac{1}{2}\overline{u_3^2}(0)$, i.e. when the turbulent potential energy is equal to the vertical turbulent kinetic energy initially, we obtain

$$\overline{\rho u_3}(\infty) = 0, \quad \overline{u_1^2}(\infty) = \overline{u_2^2}(\infty) = \tfrac{23}{24}\overline{u_1^2}(0), \quad \overline{u_3^2}(\infty) = \tfrac{5}{6}\overline{u_1^2}(0), \quad \overline{\rho^2}(\infty) = \tfrac{5}{4}N^2\overline{u_1^2}(0). \tag{3.26}$$

Since the steepest descents give a good approximation (Hinch 1991) even for finite times and the oscillation decays with time, (3.25) and (3.26) can be compared with the values at $2 \leqslant Nt \leqslant 10$ obtained directly from (3.19)–(3.22) by averaging over several oscillation periods (see figure 1).

4. Effects of viscosity and diffusion

4.1. *Spectra*

We next consider the same problem with viscosity and diffusion. The solution of (2.1)–(2.5) gives $\hat{u}_i$ ($i = 1, 2, 3$) and $\hat{\rho}$ as

$$\hat{\rho} = A\mathrm{e}^{q_1 t} + B\mathrm{e}^{q_2 t}, \tag{4.1}$$

$$\hat{u}_1 = \mathrm{e}^{-\nu k^2 t}\left\{\hat{u}_{10} + \frac{k_1 k_3}{k^2}\left[\frac{A}{q_1 + \nu k^2}\left(\mathrm{e}^{(q_1+\nu k^2)t} - 1\right) + \frac{B}{q_2 + \nu k^2}\left(\mathrm{e}^{(q_2+\nu k^2)t} - 1\right)\right]\right\}, \tag{4.2}$$

$$\hat{u}_2 = \mathrm{e}^{-\nu k^2 t}\left\{\hat{u}_{20} + \frac{k_2 k_3}{k^2}\left[\frac{A}{q_1 + \nu k^2}\left(\mathrm{e}^{(q_1+\nu k^2)t} - 1\right) + \frac{B}{q_2 + \nu k^2}\left(\mathrm{e}^{(q_2+\nu k^2)t} - 1\right)\right]\right\}, \tag{4.3}$$

$$\hat{u}_3 = \frac{1}{N^2}\left[(q_1 + \kappa k^2)A\mathrm{e}^{q_1 t} + (q_2 + \kappa k^2)B\mathrm{e}^{q_2 t}\right], \tag{4.4}$$

where

$$q_1 = \tfrac{1}{2}\left\{-(\nu + \kappa)k^2 + [(\nu - \kappa)^2 k^4 - 4a^2]^{1/2}\right\}, \tag{4.5}$$

$$q_2 = \tfrac{1}{2}\left\{-(\nu + \kappa)k^2 - [(\nu - \kappa)^2 k^4 - 4a^2]^{1/2}\right\}, \tag{4.6}$$

$$A = \frac{1}{q_2 - q_1}\left[(q_2 + \kappa k^2)\hat{\rho}_0 - N^2\hat{u}_{30}\right], \tag{4.7}$$

$$B = \frac{1}{q_1 - q_2}\left[(q_1 + \kappa k^2)\hat{\rho}_0 - N^2\hat{u}_{30}\right], \tag{4.8}$$

and a is given by (3.5).

The above solutions are valid when $(\nu-\kappa)^2k^4-4a^2\neq 0$. When $(\nu-\kappa)^2k^4-4a^2=0$, separate treatment is necessary since the case of $(\nu-\kappa)^2k^4-4a^2=0$ corresponds to the degeneration of the eigenvalues of the linear system (2.1) and (2.2). However, we see later that this is unnecessary in practice, so we do not show the results here. Using (4.1)–(4.4), we can calculate the three-dimensional spectral functions. The density–vertical velocity cospectrum is

$$\begin{aligned}\Phi_{\rho 3}(\boldsymbol{k},t) &= \tfrac{1}{2}\overline{\hat{\rho}^*\hat{u}_3+\hat{\rho}\hat{u}_3^*}\\ &= \frac{1}{\alpha^2}\left\{\sin^2\theta[-(\nu-\kappa)k^2(1-\cos\alpha t)-\alpha\sin\alpha t]\Phi_{\rho\rho}(\boldsymbol{k},0)\right.\\ &\quad\left.+N^2[-(\nu-\kappa)k^2(1-\cos\alpha t)+\alpha\sin\alpha t]\Phi_{33}(\boldsymbol{k},0)\right\}\mathrm{e}^{-(\nu+\kappa)k^2t},\end{aligned}\tag{4.9}$$

where

$$\alpha=\left(4N^2\sin^2\theta-(\nu-\kappa)^2k^4\right)^{1/2}.\tag{4.10}$$

When α is pure imaginary, we should use

$$\cos(\alpha t)=\cosh(\mathrm{i}\alpha t),\quad \sin(\alpha t)=\frac{1}{\mathrm{i}}\sinh(\mathrm{i}\alpha t),\tag{4.11}$$

in (4.9) and it becomes

$$\begin{aligned}\Phi_{\rho 3}(\boldsymbol{k},t) &= \frac{1}{\beta^2}\left\{\sin^2\theta[-(\nu-\kappa)k^2(\cosh\beta t-1)-\beta\sinh\beta t]\Phi_{\rho\rho}(\boldsymbol{k},0)\right.\\ &\quad\left.+N^2[-(\nu-\kappa)k^2(\cosh\beta t-1)+\beta\sinh\beta t]\Phi_{33}(\boldsymbol{k},0)\right\}\mathrm{e}^{-(\nu+\kappa)k^2t},\end{aligned}\tag{4.12}$$

where $\beta=\mathrm{i}\alpha$.

Note also that $\Phi_{\rho 3}(\boldsymbol{k},t)$ asymptotes to a finite value in the limit of $\alpha\to 0$ or $\beta\to 0$. In these limits both (4.9) and (4.12) become

$$\begin{aligned}\Phi_{\rho 3}(\boldsymbol{k},t) &= \left\{\sin^2\theta\left[-\tfrac{1}{2}(\nu-\kappa)k^2t^2-t\right]\Phi_{\rho\rho}(\boldsymbol{k},0)\right.\\ &\quad\left.+N^2\left[-\tfrac{1}{2}(\nu-\kappa)k^2t^2+t\right]\Phi_{33}(\boldsymbol{k},0)\right\}\mathrm{e}^{-(\nu+\kappa)k^2t},\end{aligned}\tag{4.13}$$

which means that $\Phi_{\rho 3}(\boldsymbol{k},t)$ has no singularities. The case of $\alpha=0$ or $\beta=0$ corresponds to the degeneration of the eigenvalues of the linear system (2.1) and (2.2). Since (4.12) and (4.13) agree with those obtained independently by considering from the beginning the sign of $4N^2\sin^2\theta-(\nu-\kappa)^2k^4$ in solving (2.1)–(2.5), we use henceforth a single form such as (4.9) for the expressions for $\Phi_{\rho 3}(\boldsymbol{k},t)$ and similar functions. The expressions like (4.12) or (4.13) can be recovered by using the relation (4.11) or taking the limit of $\alpha\to 0$.

Other spectrum functions can be obtained similarly but we note here a useful relation between those functions, which can be directly derived from (2.1) and (2.2). They are

$$\left(\frac{\mathrm{d}}{\mathrm{d}t}+2\nu k^2\right)\Phi_{ij}=\left(\frac{k_ik_3}{k^2}-\delta_{i3}\right)\Phi_{\rho j}+\left(\frac{k_jk_3}{k^2}-\delta_{j3}\right)\Phi_{\rho i},\tag{4.14}$$

$$\left(\frac{\mathrm{d}}{\mathrm{d}t}+(\nu+\kappa)k^2\right)\Phi_{\rho i}=\left(\frac{k_ik_3}{k^2}-\delta_{i3}\right)\Phi_{\rho\rho}+N^2\Phi_{i3},\tag{4.15}$$

$$\left(\frac{\mathrm{d}}{\mathrm{d}t}+2\nu k^2\right)\sum_i\Phi_{ii}=-2\Phi_{\rho 3},\tag{4.16}$$

$$\left(\frac{\mathrm{d}}{\mathrm{d}t}+2\kappa k^2\right)\Phi_{\rho\rho}=2N^2\Phi_{\rho 3},\tag{4.17}$$

where relations essentially identical to (4.16) and (4.17) have been previously derived by Townsend (1976). The last two can be coupled to derive an equation for the energy conservation:

$$\left(\frac{\mathrm{d}}{\mathrm{d}t}+2\nu k^2\right)\frac{1}{2}\sum_i \Phi_{ii}+\left(\frac{\mathrm{d}}{\mathrm{d}t}+2\kappa k^2\right)\frac{1}{2N^2}\Phi_{\rho\rho}=0. \tag{4.18}$$

These relations can be used to derive other three-dimensional spectrum functions from $\Phi_{\rho 3}$. Relation (4.14) can be used to derive Φ_{33} and (4.17) can be used to derive $\Phi_{\rho\rho}$; (4.16) can be used to derive $\Phi_{11}+\Phi_{22}$. To be explicit $\Phi_{\rho\rho}$ and Φ_{33} are obtained as

$$\begin{aligned}\Phi_{\rho\rho}(\boldsymbol{k},t)=\frac{2}{\alpha^2}\{&\Phi_{\rho\rho}(\boldsymbol{k},0)\left[N^2\sin^2\theta(1+\cos\alpha t)-\tfrac{1}{2}(\nu-\kappa)^2k^4\cos\alpha t\right.\\&\left.+\tfrac{1}{2}(\nu-\kappa)k^2\alpha\sin\alpha t\right]+\Phi_{33}(\boldsymbol{k},0)N^4(1-\cos\alpha t)\}\,\mathrm{e}^{-(\nu+\kappa)k^2t},\end{aligned} \tag{4.19}$$

and

$$\begin{aligned}\Phi_{33}(\boldsymbol{k},t)=-\frac{2}{\alpha^2}\{&\Phi_{\rho\rho}(\boldsymbol{k},0)\sin^4\theta(\cos\alpha t-1)+\Phi_{33}(\boldsymbol{k},0)\left[-N^2\sin^2\theta(1+\cos\alpha t)\right.\\&\left.+\tfrac{1}{2}(\nu-\kappa)^2k^4\cos\alpha t+\tfrac{1}{2}(\nu-\kappa)k^2\alpha\sin\alpha t\right]\}\,\mathrm{e}^{-(\nu+\kappa)k^2t}.\end{aligned} \tag{4.20}$$

If we assume here again initial isotropy, substitution of (3.11) and (3.12) into (4.9) gives

$$\begin{aligned}\Phi_{\rho 3}(\boldsymbol{k},t)=\frac{N^2\sin^2\theta}{4\pi k^2\alpha^2}&\left[-(\nu-\kappa)k^2(1-\cos\alpha t)\,(E(k)+2S(k))\right.\\&\left.+\alpha\sin\alpha t\,(E(k)-2S(k))\right]\mathrm{e}^{-(\nu+\kappa)k^2t}.\end{aligned} \tag{4.21}$$

4.2. *Variances and covariances*

From (4.21), the vertical density flux (assuming that the initial turbulence is isotropic) is given in terms of the initial spectrum as

$$\begin{aligned}\overline{\rho u_3}\ (t)=\frac{N^2}{2}&\int_0^\infty \mathrm{d}k\mathrm{e}^{-(\nu+\kappa)k^2t}\int_0^\pi \mathrm{d}\theta\frac{\sin^3\theta}{\alpha^2}\\&\times\left[-(\nu-\kappa)k^2(1-\cos\alpha t)\,(E(k)+2S(k))+\alpha\sin\alpha t\,(E(k)-2S(k))\right].\end{aligned} \tag{4.22}$$

In the integration of (4.22), we have to use (4.11) or take the limit of $\alpha\to 0$ in the integrand where $\alpha^2\leqslant 0$. Other covariances are given by

$$\begin{aligned}\overline{\rho^2}(t)=N^2&\int_0^\infty \mathrm{d}k\mathrm{e}^{-(\nu+\kappa)k^2t}\int_0^\pi \mathrm{d}\theta\frac{\sin\theta}{\alpha^2}\\&\times\{N^2\sin^2\theta\,[(E(k)+2S(k))-(E(k)-2S(k))\cos\alpha t]\\&-S(k)\left[(\nu-\kappa)^2k^4\cos\alpha t-(\nu-\kappa)k^2\alpha\sin\alpha t\right]\},\end{aligned} \tag{4.23}$$

and

$$\begin{aligned}\overline{u_3^2}(t)=&\int_0^\infty \mathrm{d}k\mathrm{e}^{-(\nu+\kappa)k^2t}\int_0^\pi \mathrm{d}\theta\frac{\sin^3\theta}{\alpha^2}\\&\times\{N^2\sin^2\theta\,[(E(k)+2S(k))+(E(k)-2S(k))\cos\alpha t]\\&-E(k)\left[\tfrac{1}{2}(\nu-\kappa)^2k^4\cos\alpha t+\tfrac{1}{2}(\nu-\kappa)k^2\alpha\sin\alpha t\right]\}.\end{aligned} \tag{4.24}$$

Then we obtain the normalized vertical density flux as $\overline{\rho u_3}/(\overline{\rho^2}^{1/2}\overline{u_3^2}^{1/2})(t)$.

The one-dimensional spectrum in the x-direction corresponding to (4.21) and (4.22) can be calculated as

$$\Theta_{\rho 3}(k_1,t) = \int_0^\infty r\mathrm{d}r \int_0^{2\pi} \mathrm{d}\varphi \Phi_{\rho 3}(\boldsymbol{k},t)$$

$$= \int_0^\infty \mathrm{d}r \frac{N^2}{4\pi\left(k_1^2+r^2\right)^2} \mathrm{e}^{-(\nu+\kappa)(k_1^2+r^2)t} \int_0^{2\pi} \mathrm{d}\varphi \frac{k_1^2+r^2\cos^2\varphi}{\alpha^2}$$

$$\times \left\{-(\nu-\kappa)\left(k_1^2+r^2\right)(1-\cos\alpha t)\left[E\left((k_1^2+r^2)^{1/2}\right)+2S\left((k_1^2+r^2)^{1/2}\right)\right]\right.$$

$$\left. + \alpha \sin\alpha t \left[E\left((k_1^2+r^2)^{1/2}\right)-2S\left((k_1^2+r^2)^{1/2}\right)\right]\right\}, \tag{4.25}$$

with

$$\alpha = \left(\frac{4N^2\left(k_1^2+r^2\cos^2\varphi\right)-(\nu-\kappa)^2\left(k_1^2+r^2\right)^3}{k_1^2+r^2}\right)^{1/2}, \tag{4.26}$$

where (r,φ) denotes cylindrical coordinates; k_1 is the wavenumber in the x-direction, r is the radial distance from the x-axis and φ is the azimuthal angle measured around the x-axis.

An important feature of the three-dimensional spectral function (4.21) is that, when $Pr > 1$ (so that $\nu - \kappa > 0$), the viscous and diffusive effects act to induce the countergradient flux at high wavenumber k because of the term containing $-(\nu-\kappa)k^2$. On the other hand, when $Pr < 1$ (i.e. $\nu-\kappa < 0$), the viscous and diffusive effects act to prevent the countergradient flux at high wavenumber. The covariance $\overline{\rho u_3}(t)$ given by (4.22) has the same feature. This explains why the water tank experiments for $Pr > 1$ ($Pr = 6$ (thermal stratification), $Pr = 600$ (salt stratification), e.g. Itsweire *et al.* 1986; Komori & Nagata 1995) often show a stronger countergradient flux than the wind tunnel experiments ($Pr = 0.7 < 1$) (e.g. Lienhard & Van Atta 1990). We should note that the initial isotropy assumed in (4.21) and thereafter is *not* essential to this result since the general three-dimensional spectrum function (4.9) has the same character. In DNS, Gerz & Yamazaki (1993) found in their three-dimensional spectra a persistent countergradient flux at high radial wavenumber when $Pr = 2$, but did not observe it when $Pr = 1$ (see their figure 14). When $Pr = 1$, α becomes simply $\alpha = 2N\sin\theta$ and (4.21) oscillates like $\sin(2Nt\sin\theta)$, with no dependence on the radial wavenumber k. This shows that all the radial wavenumber components oscillate in phase.

To see the special character of the turbulence when $Pr = 1$ (i.e. $\nu - \kappa = 0$) we write the covariances in this case explicitly:

$$\overline{\rho u_3}(t) = \frac{N}{4}\int_0^\infty \mathrm{d}k\,(E(k)-2S(k))\,\mathrm{e}^{-2\nu k^2 t}\int_0^\pi \mathrm{d}\theta \sin^2\theta \sin(2Nt\sin\theta), \tag{4.27}$$

$$\overline{\rho^2}(t) = \frac{N^2}{4}\left[\int_0^\infty \mathrm{d}k\,2\,(E(k)+2S(k))\,\mathrm{e}^{-2\nu k^2 t}\right.$$

$$\left. - \int_0^\infty \mathrm{d}k\,(E(k)-2S(k))\,\mathrm{e}^{-2\nu k^2 t}\int_0^\pi \mathrm{d}\theta \sin\theta\cos(2Nt\sin\theta)\right], \tag{4.28}$$

and

$$\overline{u_1^2}(t) = \overline{u_2^2}(t)$$
$$= \int_0^\infty \mathrm{d}k \left(\tfrac{7}{12}E(k) + \tfrac{1}{6}S(k)\right) \mathrm{e}^{-2\nu k^2 t}$$
$$+ \frac{1}{8}\int_0^\infty \mathrm{d}k\,(E(k) - 2S(k))\,\mathrm{e}^{-2\nu k^2 t} \int_0^\pi \mathrm{d}\theta \cos^2\theta \sin\theta \cos(2Nt\sin\theta), \quad (4.29)$$

$$\overline{u_3^2}(t) = \frac{1}{4}\left[\int_0^\infty \mathrm{d}k \tfrac{4}{3}(E(k) + 2S(k))\,\mathrm{e}^{-2\nu k^2 t}\right.$$
$$\left. + \int_0^\infty \mathrm{d}k\,(E(k) - 2S(k))\,\mathrm{e}^{-2\nu k^2 t} \int_0^\pi \mathrm{d}\theta \sin^3\theta \cos(2Nt\sin\theta)\right]. \quad (4.30)$$

The oscillation periods of these functions are independent of the initial condition $E(k)$ and $S(k)$. They do not depend even on KE_0 and PE_0. They are determined only by the integrals such as

$$\int_0^\pi \mathrm{d}\theta \sin^2\theta \sin(2Nt\sin\theta), \quad (4.31)$$

which are identical to those that determine the time development of the inviscid flux (3.19)–(3.22). Then the zeros of the vertical density flux $\overline{\rho u_3}(t)$, which correspond to the onset and disappearance of countergradient flux, agree with the inviscid result. Many studies using DNS have focused on the case of $Pr = 1$ (e.g. Riley *et al.* 1981, Métais & Herring 1989; Gerz & Yamazaki 1993). Our analysis shows that this case has rather special properties. The zeros for air-flow experiments, where $Pr = 0.7$, display similar results to those for $Pr = 1$. This explains why in many previous studies, the time at which the vertical flux vanishes does not show much sensitivity to the initial conditions. The amplitude of the oscillation is determined by $E(k) - 2S(k)$, so that the time oscillation vanishes if $E(k) = 2S(k)$.

What is interesting in the 'normalized' vertical density flux $\overline{\rho u_3}/(\overline{\rho^2}^{1/2}\overline{u_3^2}^{1/2})(t)$ is that, when $Pr = 1$ and also $E(k)$ and $S(k)$ have the same form except for the multiplying constant, the normalized flux becomes exactly identical to the inviscid flux. As we see from (4.27), (4.28) and (4.30), if $S(k)$ is proportional to $E(k)$, i.e. $S(k) = CE(k)$ and C is a constant ($= PE_0/KE_0 \geqslant 0$), the integrals over k are cancelled out in deriving the normalized flux. Then the flux becomes identical to the inviscid flux calculated from (3.19), (3.21) and (3.22) assuming $PE_0 = CKE_0$:

$$\frac{\overline{\rho u_3}}{\overline{\rho^2}^{1/2}\overline{u_3^2}^{1/2}} = \frac{(1-2C)\displaystyle\int_0^\pi \mathrm{d}\theta \sin^2\theta \sin(2Nt\sin\theta)}{\left[2(1+2C) - (1-2C)\displaystyle\int_0^\pi \mathrm{d}\theta \sin\theta\cos(2Nt\sin\theta)\right]^{1/2}}$$
$$\times \frac{1}{\left[\frac{4}{3}(1+2C) + (1-2C)\displaystyle\int_0^\pi \mathrm{d}\theta \sin^3\theta\cos(2Nt\sin\theta)\right]^{1/2}}. \quad (4.32)$$

When $E(k) = 0$ (i.e. $KE_0 = 0$), the normalized flux again agrees with the inviscid flux

and it becomes

$$\frac{\overline{\rho u_3}}{\overline{\rho^2}^{1/2}\overline{u_3^2}^{1/2}} = -\frac{\displaystyle\int_0^\pi \mathrm{d}\theta \sin^2\theta \sin(2Nt\sin\theta)}{\left[2+\displaystyle\int_0^\pi \mathrm{d}\theta \sin\theta\cos(2Nt\sin\theta)\right]^{1/2}\left[\frac{4}{3}-\displaystyle\int_0^\pi \mathrm{d}\theta \sin^3\theta\cos(2Nt\sin\theta)\right]^{1/2}}, \tag{4.33}$$

which is consistent with (4.32) in the limit of $C \to \infty$.

In these cases, we can examine the purely nonlinear effects (without the effects of viscosity/diffusion) by comparing the normalized flux of RDT with those of DNS and laboratory experiments, or more generally, by considering the non-dimensional 'ratios' of the covariances, including the anisotropy tensor (see figure 4 of §5). In laboratory experiments, the initial normalized flux is usually zero, implying neither $KE_0 = 0$ nor $PE_0 = 0$. As we have seen in §3.2, if $PE_0 = 0$, the initial normalized flux should be $\overline{\rho u_3}/(\overline{\rho^2}^{1/2}\overline{u_3^2}^{1/2})(t \to 0) = 1 \neq 0$, and if $KE_0 = 0$, it should be $\overline{\rho u_3}/(\overline{\rho^2}^{1/2}\overline{u_3^2}^{1/2})(t \to 0) = -(5/6)^{1/2} = -0.913 \neq 0$. On the other hand, the main results of DNS by Gerz & Yamazaki (1993) (their cases A, B, C and H) and some of the results by Métais & Herring (1989) are for $Pr = 1$ with $KE_0 = 0$ or $PE_0 = 0$. Their results, which correspond to these cases, are compared with our RDT results in §5.

The one-dimensional cospectrum given by (4.25) shows that, when $Pr > 1$ (i.e. $\nu - \kappa > 0$), the viscous and diffusive effects act to enforce the countergradient flux at high wavenumber k_1. On the other hand, when $Pr < 1$, the viscous and diffusive effects act to reduce the countergradient at high wavenumber. However, (4.25) has a rather complicated form and when $Pr = 1$ it becomes

$$\Theta_{\rho 3}\ (k_1,t) = \frac{N}{8\pi}\int_0^\infty \mathrm{d}r \frac{1}{\left(k_1^2+r^2\right)^2}\mathrm{e}^{-2\nu\left(k_1^2+r^2\right)t}\int_0^{2\pi}\mathrm{d}\varphi\left(k_1^2+r^2\right)^{1/2}\left(k_1^2+r^2\cos^2\varphi\right)^{1/2}$$
$$\times\sin\left(2Nt\frac{\left(k_1^2+r^2\cos^2\varphi\right)^{1/2}}{\left(k_1^2+r^2\right)^{1/2}}\right)\left[E\left((k_1^2+r^2)^{1/2}\right)-2S\left((k_1^2+r^2)^{1/2}\right)\right]. \tag{4.34}$$

The effect of Pr is not straightforward. Even when $Pr = 1$, calculation of (4.34) shows the appearance of a countergradient flux at high wavenumbers. Since $(k_1^2+r^2\cos^2\varphi)^{1/2}/(k_1^2+r^2)^{1/2}$ increases monotonically with k_1, the oscillation period is smaller for larger k_1. This is the reason why the high-wavenumber components 'become countergradient' sooner. Note that this does not lead to the countergradient flux which is 'persistently localized' at high wavenumbers. This is merely a transitory countergradient flux at high wavenumbers. We consider this problem again in §5 (figure 6).

The short-time approximations ($t \ll 1$) of the covariances in the presence of viscous and diffusive effects give the same results as for the inviscid theory at the leading order. For the calculation of the long-time approximations ($t \gg 1$) of the density variance, we first rewrite (4.23) in the following form:

$$\overline{\rho^2}(t) = N^2\int_0^{\left(\frac{2N}{|\nu-\kappa|}\right)^{1/2}}\mathrm{d}k\int_0^\pi \mathrm{d}\theta \mathrm{e}^{-(\nu+\kappa)k^2t}\frac{\sin\theta}{\alpha^2}N^2\sin^2\theta\,(E(k)+2S(k))^{(I)}$$
$$+N^2\int_{\left(\frac{2N}{|\nu-\kappa|}\right)^{1/2}}^\infty \mathrm{d}k\int_0^\pi \mathrm{d}\theta \mathrm{e}^{-(\nu+\kappa)k^2t}\frac{\sin\theta}{\alpha^2}N^2\sin^2\theta\,(E(k)+2S(k))^{(II)}$$

$$+N^2\int_0^{\left(\frac{2N}{|\nu-\kappa|}\right)^{1/2}}\mathrm{d}k\int_{\theta_1}^{\theta_2}\mathrm{d}\theta \mathrm{e}^{-(\nu+\kappa)k^2t}\sin\theta\left\{-N^2\sin^2\theta\,(E(k)-2S(k))\frac{\cos\alpha t^{(III)}}{\alpha^2}\right.$$
$$\left.-S(k)\left[(\nu-\kappa)^2k^4\frac{\cos\alpha t^{(IV)}}{\alpha^2}-(\nu-\kappa)k^2\frac{\sin\alpha t^{(V)}}{\alpha}\right]\right\}$$
$$+N^2\int_0^{\pi}\mathrm{d}\theta\int_{\left(\frac{2N\sin\theta}{|\nu-\kappa|}\right)^{1/2}}^{\infty}\mathrm{d}k\mathrm{e}^{-(\nu+\kappa)k^2t}\sin\theta\left\{N^2\sin^2\theta\,(E(k)-2S(k))\frac{\cosh\beta t^{(VI)}}{\beta^2}\right.$$
$$\left.+S(k)\left[(\nu-\kappa)^2k^4\frac{\cosh\beta t^{(VII)}}{\beta^2}+(\nu-\kappa)k^2\frac{\sinh\beta t^{(VIII)}}{\beta}\right]\right\}, \tag{4.35}$$

where

$$\beta=\mathrm{i}\alpha, \tag{4.36}$$

and

$$\theta_1=\cos^{-1}b\quad\left(0\leqslant\theta\leqslant\frac{\pi}{2}\right),\qquad\theta_2=\cos^{-1}(-b)\quad\left(\frac{\pi}{2}\leqslant\theta\leqslant\pi\right), \tag{4.37}$$

with

$$b=\left(1-\frac{(\nu-\kappa)^2k^4}{4N^2}\right)^{1/2}. \tag{4.38}$$

In the first and second integrals of (4.35), i.e. the terms with superscript (*I*) and (*II*), the dominant contribution to the integral comes from $k\to 0$. In the third integral (terms (*III*)–(*V*)), the dominant contribution comes from the dual limit of $k\to 0$ and $\theta\to\pi/2$. In the forth integral (terms (*VI*)–(*VIII*)) the dominant contribution comes from the dual limit of $k\to k_0$ and $\theta\to 0,\ \pi$, where k_0 is given by

$$k_0=\left(\frac{N^2\sin^2\theta\,(\nu+\kappa)^2}{\nu\kappa\,|\nu-\kappa|^2}\right)^{1/4}. \tag{4.39}$$

If we assume that $E(k)$ and $S(k)$ near $k=0$, which must be of even order of k, have the same form except the multiplying constant:

$$E(k)=a_Ek^{2l}\ (l\geqslant 1,\ l:\text{integer}), \tag{4.40}$$

$$S(k)=a_Sk^{2l}\ (l\geqslant 1,\ l:\text{integer}), \tag{4.41}$$

the term with superscript (*I*) decays like $\propto t^{-(l+1/2)}$ in the long-time limit ($t\to\infty$), the term with superscript (*II*) decays exponentially with time, the term with superscript (*III*) decays like $\propto t^{-(l+1)}$, the term with superscript (*IV*) decays like $\propto t^{-(l+3)}$, the term with superscript (*V*) decays like $\propto t^{-(l+2)}$ and the terms with superscripts (*VI*),(*VII*) and (*VIII*) decay like $\propto t^{-(l+5/2)}$.

Then the dominant term in the long-time limit is the first integral with superscript (*I*) and the result is

$$\overline{\rho^2}(t)=\frac{N^2}{2}(a_E+2a_S)\frac{(2l-1)!!\pi^{1/2}}{2^{l+1}(\nu+\kappa)^{l+1/2}t^{l+1/2}}\quad(t\gg 1). \tag{4.42}$$

The values of $\overline{u_3^2}$ and $\overline{\rho u_3}$ can be calculated similarly as

$$\overline{u_3^2}(t)=\tfrac{1}{3}(a_E+2a_S)\frac{(2l-1)!!\pi^{1/2}}{2^{l+1}(\nu+\kappa)^{l+1/2}t^{l+1/2}}\quad(t\gg 1), \tag{4.43}$$

and

$$\overline{\rho u_3}(t) = (a_E - 2a_S)\frac{(2l-1)!!N^{1/2}\pi}{2^{l+3}(\nu+\kappa)^{l+1/2}t^{l+1}}\sin\left(2Nt - \frac{\pi}{4}\right) \quad (t \gg 1). \tag{4.44}$$

These results show that, if $E(k), S(k) \propto k^2$ in the limit of $k \to 0$ (i.e. if $l = 1$) as noted by Saffman (1967), we obtain

$$\overline{\rho^2}, \overline{u_3^2} \propto t^{-3/2}, \quad \overline{\rho u_3} \propto t^{-2}, \tag{4.45}$$

and if $E(k), S(k) \propto k^4$ in the limit of $k \to 0$ (i.e. if $l = 2$) (cf. Batchelor & Proudman, 1956) as used in most of the DNS of the final decay of turbulence (Riley *et al.* 1981; Métais & Herring 1989; Gerz & Yamazaki 1993),

$$\overline{\rho^2}, \overline{u_3^2} \propto t^{-5/2}, \quad \overline{\rho u_3} \propto t^{-3}. \tag{4.46}$$

From (4.42), (4.43) and (4.44) we note that the normalized vertical density flux in the long-time limit becomes

$$\frac{\overline{\rho u_3}}{\overline{\rho^2}^{1/2}\overline{u_3^2}^{1/2}} = \frac{(a_E - 2a_S)}{(a_E + 2a_S)}\frac{(6\pi)^{1/2}}{4N^{1/2}t^{1/2}}\sin\left(2Nt - \frac{\pi}{4}\right), \tag{4.47}$$

irrespective of the forms of $E(k)$ and $S(k)$ near $k = 0$. It shows a decaying oscillation with decay rate $t^{-1/2}$ and an oscillation period π/N. Even when $E(k)$ and $S(k)$ have different functional forms near $k = 0$, we can still use (4.47) by substituting $a_E = 0$ if $E(k)$ decays faster than $S(k)$ near $k = 0$, or by substituting $a_S = 0$ if $S(k)$ decays faster than $E(k)$ near $k = 0$. The functional form of (4.47) is the same as the inviscid normalized flux (which is easily derived from the results of §3) except for the multiplying constant. Thus the normalized vertical density flux $\overline{\rho u_3}/(\overline{\rho^2}^{1/2}\overline{u_3^2}^{1/2})$ in the long-time limit always shows a decaying oscillation with decay rate $t^{-1/2}$ and an oscillation period π/N, irrespective of any initial conditions at least in so far as the turbulence is initially isotropic.

We see from (4.42) and (4.43) that, in the long-time limit ($t \to \infty$), the ratio of the potential energy to the vertical kinetic energy becomes

$$ER \equiv \frac{(1/2N^2)\overline{\rho^2}}{\frac{1}{2}\overline{u_3^2}} = \frac{3}{2}. \tag{4.48}$$

As discussed in §3, this value is identical with the inviscid result and broadly agrees with the existing observations, experiments and LES results. Note that the result holds independently of the Prandtl number Pr, Reynolds number Re, Froude number Fr and the initial conditions (other than the important assumption of initial isotropy). Although the results (4.42) and (4.43) depend on the functional forms of $E(k)$ and $S(k)$ near $k = 0$, the ratio (4.48) does not depend on these functional forms. Even when $E(k)$ and $S(k)$ have different forms, the one which shows slower decay as $k \to 0$ (i.e. $\propto k^{2l}$ ($k \to 0$) with smaller l) gives the main contribution to (4.42) and (4.43). The ratio (4.48) is independent of $E(k)$ and $S(k)$. An alternative explanation is that, in the long-time limit $\overline{\rho^2}(t)$ given by (4.35) is dominated by the first term with superscript (I), and the main contribution to the integral comes from near $k = 0$. Then, $\overline{\rho^2}$ is approximated by

$$\frac{N^2}{2}\int_0^\infty \mathrm{d}k \mathrm{e}^{-(\nu+\kappa)k^2 t}(E(k) + 2S(k)) \quad (t \gg 1). \tag{4.49}$$

The corresponding leading term in $\overline{u_3^2}$ is

$$\frac{1}{3}\int_0^\infty \mathrm{d}k \mathrm{e}^{-(\nu+\kappa)k^2 t}\,(E(k)+2S(k))\ (t\gg 1). \tag{4.50}$$

If we take the ratio of these leading terms, the integrals are cancelled irrespective of the forms of $E(k)$ and $S(k)$, leading to (4.48). In (4.49) and (4.50), the integrand has the same form as the steady part of the corresponding inviscid covariances, except the exponentially decaying factor $\mathrm{e}^{-(\nu+\kappa)k^2 t}$. This is the reason why the viscous/diffusive and the inviscid results give the same ratio (4.48).

For large Prandtl number ($Pr\gg 1$) flow, Pearson & Linden (1983) noted under the condition $N\sin\theta/\{(\nu-\kappa)k^2\}\ll 1$ that the mode corresponding to q_1 decays more slowly than the mode of q_2. Here q_1 and q_2 are the eigenvalues of the linear system (2.1) and (2.2), as given in (4.5) and (4.6). In usual laboratory experiments performed in an apparatus with a finite horizontal size D, there is a minimum in the horizontal wavenumber k_H which is given by $k_{Hmin}=2\pi/D$. In such cases one vertical wavenumber decays most slowly, namely $k_3=(2N^2k_{Hmin}^2/\nu\kappa)^{1/6}$. This result can be obtained by seeking the wavenumber which makes $|q_1|$ minimum under the three prescribed restrictions, i.e. $Pr\gg 1$, $N\sin\theta/\{(\nu-\kappa)k^2\}\ll 1$ and $k_{Hmin}=2\pi/D$. Although they did not calculate the fluxes and did not consider the integrated effects over k-space, this theoretical vertical scale was in good agreement with the experiments by Linden (1980).

It is of interest to note that in the fourth integral of (4.35), i.e. in the (*VI*), (*VII*) and (*VIII*) terms, the main contribution comes from the wavenumber components given by (4.39). In the limit of $Pr\gg 1$, this value of k_0 agrees with that of the 'most slowly decaying mode' given by Pearson & Linden (1983) (see their equation (12)). The main contribution to the fourth integral comes from the coexisting limit of $\sin\theta=k_H/k\to 0$ as we have shown already, indicating that this integral shows the decay in horizontal layers as observed by Pearson & Linden (1983). The integral contains only the contribution from imaginary α (high-wavenumber components which satisfy $N\sin\theta/\{|\nu-\kappa|k^2\}<1/2$) and this is similar to the condition $N\sin\theta/\{(\nu-\kappa)k^2\}\ll 1$ assumed in Pearson & Linden (1983) along with $Pr\gg 1$. Then the integral comprises the 'generalized' conditions for the decay in horizontal layers, without strong limitations of $Pr\gg 1$ or $N\sin\theta/\{(\nu-\kappa)k^2\}\ll 1$. However, as we have seen already, this integral decays like $\propto t^{-(l+5/2)}$ in the limit of $t\to\infty$ and decays faster than the first integral of (4.35) as given by (4.42). If the flow is unbounded as is assumed in this analysis, the most slowly decaying mode has the wavenumber $k\to 0$, and the main contribution to the integral in the k-space also comes from near $k=0$ in the long-time limit. If the flow is bounded as in Pearson & Linden's (1983) experiments, the wavenumber components that contribute most become non-zero and the decay rate is different. Further analyses are necessary to assess the effect of the boundedness of the fluid. It is important to note that only the fourth integral represents the decay in horizontal layers, even if it does not decay most slowly.

It is significant that the horizontal layering occurs independent of the Prandtl number when $Pr\neq 1$. On the other hand, when $Pr=1$ ($\nu-\kappa=0$), the integration region vanishes in the fourth integral of (4.35) since $(2N\sin\theta/|\nu-\kappa|)^{1/2}\to\infty$. Indeed (4.28) is reminiscent of the first and third integrals of (4.35), which do not show a decay in horizontal layers. Thus the horizontal layering does not occur when $Pr=1$.

A striking feature of homogeneous stratified turbulence is that initially (when

$Fr \gg 1$) it decays at much the same rate as neutrally stratified turbulence (e.g. Britter *et al.* 1983). In this range, the stratification has an enormous effect on vertical diffusion. But when $Fr < 1$, it is observed that the turbulence changes into layer-like motions, as in Pearson & Linden (1983). We can explain this phenomenon by considering the change to an effective turbulent Prandtl number Pr_t based on the eddy diffusion for scalar and momentum, which can be substituted for Pr in our analysis to investigate the nonlinear effects. For neutral turbulence (i.e. $Fr_l \gg 1$) the turbulent Prandtl number satisfies $Pr_t \leqslant 1$ (Townsend 1976), while for stably stratified turbulence, when $Fr_l \leqslant 1$, $Pr_t \gg 1$. Our results described above are consistent with the observations that, in the parameter region of $Pr_t \approx 1$, as in the initial time development of the stratified turbulence, layering does not occur and the decay is largely isotropic. They also explain that, as the turbulence decays with time and Pr_t becomes larger ($Pr_t \gg 1$), the layering as observed by Pearson & Linden (1983) occurs.

Using DNS, Gerz & Yamazaki (1993) computed covariances using a coarse (64^3) and a fine (128^3) grid. They found an increasing difference over time, which reaches a maximum at $Nt/2\pi \approx 0.25$, which they explained as due to the differences in high-wavenumber components (see their figures 11 and 12*c*,*e*). However, the difference decreases again with time and at $Nt/2\pi \approx 0.5$ almost vanishes. This suggests that the contribution from low-wavenumber components becomes dominant and the differences at high wavenumbers becomes less important in the long time. Because of the periodic boundary condition, DNS can resolve the 'large' scale only to the scale of integer wavenumber 1. This leads again to the significant differences between DNS and RDT results after a further longer periods.

We finally note the behaviour of the 'quad' antiphase-spectrum $Q_{\rho 3}$. Using RDT, this can be calculated as

$$\begin{aligned} Q_{\rho 3}(\boldsymbol{k}, t) &\equiv -\frac{\mathrm{i}}{2}\overline{\hat{\rho}^* \hat{u}_3 - \hat{u}_3{}^* \hat{\rho}} \\ &= Q_{\rho 3}(\boldsymbol{k}, 0)\mathrm{e}^{-(\nu+\kappa)k^2 t}. \end{aligned} \tag{4.51}$$

This shows that, if the initial value is $Q_{\rho 3}(\boldsymbol{k}, 0) = 0$, then $Q_{\rho 3}(\boldsymbol{k}, t) = 0$ for all time. The measurement of the phase angle $\theta = \tan^{-1}(Q_{\rho 3}/\Phi_{\rho 3})$ in the experiments (figure 22 of Lienhard & Van Atta 1990; figure 16 of Yoon & Warhaft 1990) shows that initially $\theta \simeq 180°$ except at high wavenumbers where $\Phi_{\rho 3} \simeq 0$. Therefore $Q_{\rho 3}(\boldsymbol{k}, 0) \simeq 0$. Although the experiments show that θ fluctuates rapidly with the wavenumber when the vertical density flux $\overline{\rho u_3}$ vanishes, it does not necessarily mean that $Q_{\rho 3}(\boldsymbol{k}, t)$ takes large values. If the initial quad spectrum $Q_{\rho 3}(\boldsymbol{k}, 0)$, and therefore $Q_{\rho 3}(\boldsymbol{k}, t)$ have small deviations from zero, a large scatter of phase angle θ results when $\Phi_{\rho 3} \simeq 0$.

5. Comparison with DNS and experiments

Now we compare our theory with the existing direct numerical simulations and laboratory experiments. In all the examples shown below for comparison with DNS and experiments, we use an initial isotropic kinetic turbulent energy spectrum $E(k)$ which satisfies (3.13):

$$E(k) = KE_0 \left(\frac{2}{9\pi}\right)^{1/2} \left(\frac{2}{k_0}\right)^5 k^4 \mathrm{e}^{-2k^2/k_0^2}, \tag{5.1}$$

with k_0 being the peak wavenumber. For the potential energy spectrum $S(k)$ we use the same form as the kinetic energy spectrum which is given by

$$S(k) = PE_0 \left(\frac{2}{9\pi}\right)^{1/2} \left(\frac{2}{k_0}\right)^5 k^4 \mathrm{e}^{-2k^2/k_0^2}, \tag{5.2}$$

and satisfies (3.14). These spectral forms correspond to the final period of decay of turbulence and have been used in the relevant DNS for unsheared flows (Riley *et al.* 1981; Métais & Herring 1989; Gerz & Yamazaki 1993). These give $E(k), S(k) \propto k^4$ in the limit of $k \to 0$. In the experiments, $E(k), S(k) \propto k^2$ is more usual. However, the use of

$$E(k) = KE_0 \left(\frac{16}{\pi}\right)^{1/2} \frac{k^2}{k_0^3} \mathrm{e}^{-k^2/k_0^2}, \quad S(k) = PE_0 \left(\frac{16}{\pi}\right)^{1/2} \frac{k^2}{k_0^3} \mathrm{e}^{-k^2/k_0^2}, \tag{5.3}$$

which gives $E(k), S(k) \propto k^2$ ($k \to 0$) did not show qualitative differences in the subsequent results, except for the decay rate of the turbulence. Therefore, we use (5.1) and (5.2) throughout the paper for comparison with both the DNS and the experiments. Some differences due to the initial spectral forms observed in comparison with the experiments are described where appropriate.

Figure 2(*a*) shows the time development of the normalized vertical density flux obtained by Gerz & Yamazaki (1993) for $Pr = 1$. In this example the initial kinetic energy is zero ($KE_0 = 0$) and the potential energy spectrum is given by (5.2). They showed that, when the initial potential energy is large (their case B has energy 256 times larger than case C, and case A has energy 16 times larger), the flux decays faster with time and the oscillation period increases for $Nt/2\pi > 1.5$. Note here that $\overline{\rho u_3}/(\overline{\rho^2}^{1/2}\overline{u_3^2}^{1/2}) = -\overline{Tu_3}/(\overline{T^2}^{1/2}\overline{u_3^2}^{1/2})$, if the perturbation temperature T is used instead of the perturbation density. Although Gerz & Yamazaki (1993) did not give the time development of the turbulent Froude number Fr, the energy transfer spectrum decays with time and even in their most energetic case B, it decays to a very small value after $Nt/2\pi = 0.48$, showing that the nonlinear effect would be negligible after that time. Since $Pr = 1$ and $KE_0 = 0$, the fluxes obtained by RDT with viscous and diffusive effects agree with the inviscid fluxes as given by (4.33). The RDT results do not depend on the form of $S(k)$. This is shown in figure 2(*b*). Since (4.33) depends only on Nt and not on ν or κ (i.e. Re or Fr), the difference between figures 2(*a*) and 2(*b*) comes only from the nonlinear effect. Gerz & Yamazaki (1993) argued that their case C, which has the smallest turbulence energy, shows very weak nonlinearity since the oscillation period is approximately $Nt = \pi$. This is verified here by the almost complete agreement between their case C and RDT results for $Nt/2\pi < 2.5$. We see also that the amplitude agrees well. Some differences for larger times (i.e. $Nt/2\pi > 2.5$) are likely to arise because DNS cannot resolve the larger scales ($k \approx 0$) whose effect becomes dominant after a long time. We can say that the stronger decay and the increase of the period notable in cases A and B are the purely nonlinear effect due to the large turbulence energy. Gerz & Yamazaki argued, quoting a personal communication from H. Wijesekera, that the majority of turbulent patches observed in the ocean correspond to their case C, although noticeable minority correspond to their case B. Thus, case C is representative of the natural turbulence in geophysical contexts.

As has been noted in §3, the large negative initial value of the normalized flux at $t = 0$ (strong countergradient flux) given by DNS ($= -0.913$) agrees with the inviscid RDT result ($= -(5/6)^{1/2} = -0.913$). In this case the effect of viscosity/diffusion is

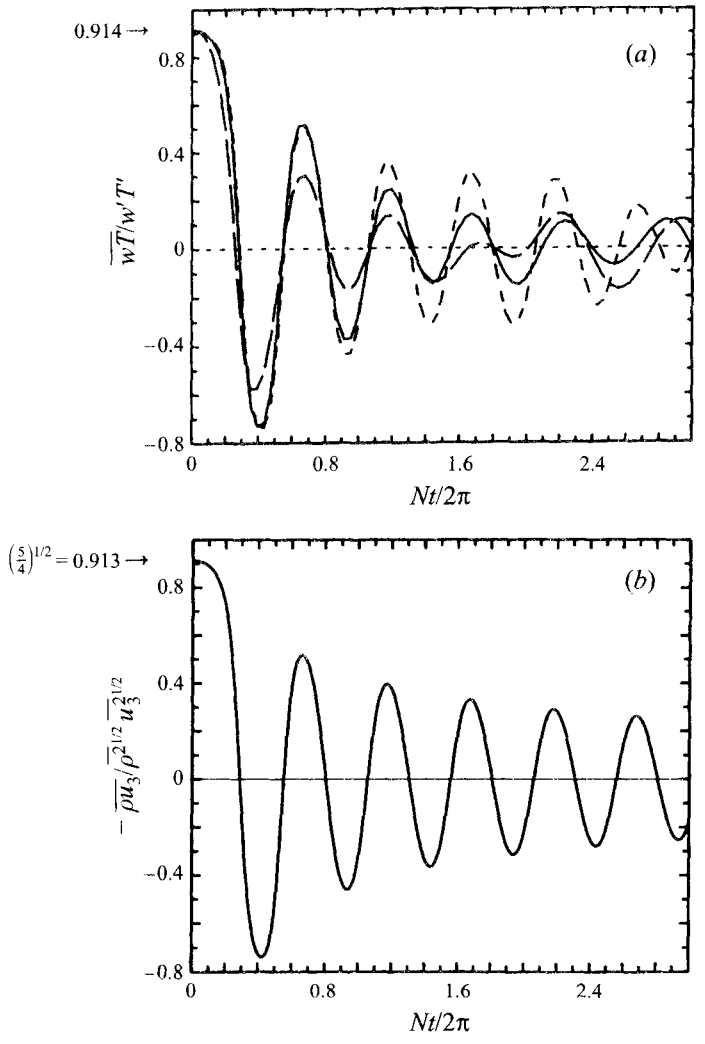

FIGURE 2. Time development of the normalized vertical density flux when $Pr = 1$ and $KE_0 = 0$. (*a*) DNS results by Gerz & Yamazaki (1993, figure 8): ————, case A ($PE_0 = 0.46$ in their units); — — — —, case B ($PE_0 = 7.37$); - - - - - -, case C ($PE_0 = 0.029$). (*b*) RDT. In DNS the nonlinear effect would be negligible when $Nt/2\pi > 0.48$.

absent even in a long-time development when the results are solely due to linear effects.

Figure 3 shows the comparison of the normalized vertical density flux obtained by RDT with the DNS results by Métais & Herring (1989). In this case $Pr = 1$ and $PE_0/KE_0 = 0.05$. In DNS the turbulent Froude number satisfies $Fr < 1$ when $Nt > 2$ (figure 7 of Métais & Herring 1989) and the RDT would be applicable for that period. In RDT we assume the same form for $E(k)$ and $S(k)$ as in (5.1) and (5.2), and the normalized flux agrees with the inviscid flux as has been shown in (4.32). The form of $E(k)$ is the same in DNS and RDT, and is given by (5.1). However, in DNS, an unstratified calculation was done before stratification was switched on at time $t = 0.685$ to match the experimental conditions. This causes a change in the 'initial' kinetic energy spectrum and leads to the uncertainty in the initial condition necessary

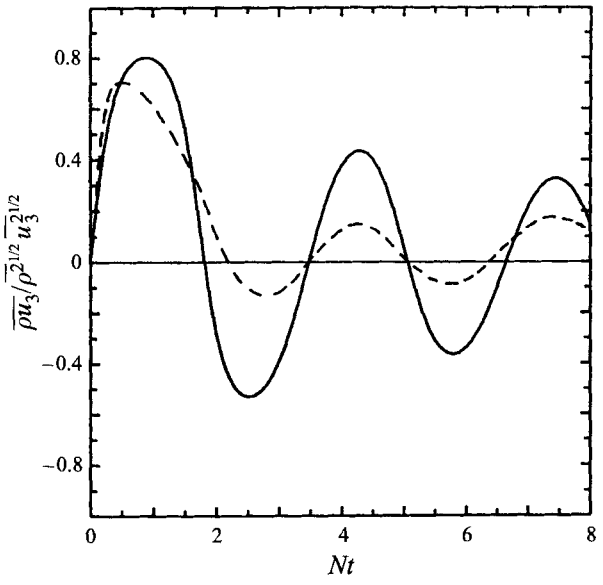

FIGURE 3. Time development of the normalized vertical density flux when $Pr = 1$ and $PE_0/KE_0 = 0.05$. — — — —, DNS by Métais & Herring (1989, figure 3); ————, RDT. In DNS $Fr < 1$ is satisfied when $Nt > 2$.

for the comparison with RDT results. Recent similar DNS by the same group (Kimura & Herring 1996) shows that, at the time when the stratification is switched on, the spectrum near $k = 0$ gives approximately $E(k) \propto k^2$ and is different from $E(k) \propto k^4$, which is given by (5.1). This difference leads to the different subsequent time development. The functional form of $S(k)$ is not explicitly given in the paper of Métais & Herring (1989). There is also an uncertainty in the spectral form of $S(k)$ used in DNS. These differences in the initial conditions make the comparison between DNS and RDT incomplete.

However, as equation (4.27) shows, the zeros of the flux are independent of $E(k)$ and $S(k)$ when $Pr = 1$, and the differences between zeros of the flux result purely from nonlinear effects. We find that third and fourth zeros agree but second and fifth zeros show some differences. On the other hand, figure 2(*a*) shows that, even when the turbulence energy is very large, the zeros agree with the RDT, at least for the first five zeros. This suggests that the difference of some zeros is not an effect of nonlinearity. The effect of some numerical errors in DNS is a plausible explanation here. We note that the initial peak value of the normalized flux agrees fairly well if we use the same PE_0/KE_0 in DNS and RDT. This illustrates the importance of the initial conditions KE_0 and PE_0 in the unsteady turbulence. The faster decay of the normalized flux in DNS would be the nonlinear effect since (4.47) shows that the decay rate in the long-time limit is independent of the initial spectrum form.

Figure 4 shows the time development of the trace components of the anisotropy tensor defined by

$$b_{ij} = \frac{\overline{u_i u_j}}{\overline{u_1^2} + \overline{u_2^2} + \overline{u_3^2}} - \frac{1}{3}. \tag{5.4}$$

When $b_{ii} = 0$ $(i = 1, 2, 3)$, the turbulence is isotropic. Figure 4(*a*), which is case C (small turbulence energy) of Gerz & Yamazaki (1993), agrees quantitatively with the RDT result given in figure 4(*b*). When $Pr = 1$ and $E(k) = 0$, the anisotropy tensor in

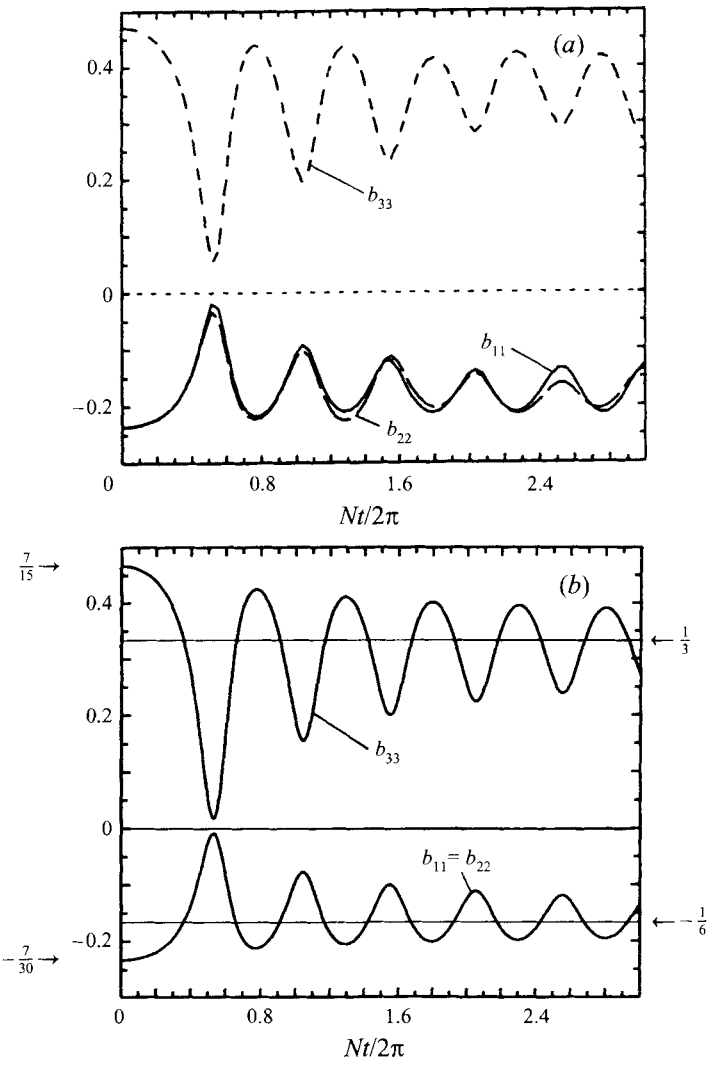

FIGURE 4. Time development of the trace components of the anisotropy tensor $b_{ii}(i = 1, 2, 3)$ when $Pr = 1$ and $KE_0 = 0$. (*a*) DNS by Gerz & Yamazaki(1993, figure 9*c*) (*b*) RDT.

RDT agrees with the inviscid result, since the integrals containing $S(k)$ are cancelled out. The trace components are

$$b_{11} = b_{22} = \frac{\frac{1}{6} - \frac{1}{4}\int_0^\pi \mathrm{d}\theta \cos^2\theta \sin\theta \cos(2Nt\sin\theta)}{1 - \frac{1}{2}\int_0^\pi \mathrm{d}\theta \cos^2\theta \sin\theta \cos(2Nt\sin\theta) - \frac{1}{2}\int_0^\pi \mathrm{d}\theta \sin^3\theta \cos(2Nt\sin\theta)} - \frac{1}{3}, \tag{5.5}$$

and

$$b_{33} = \frac{\frac{2}{3} - \frac{1}{2}\int_0^\pi \mathrm{d}\theta \sin^3\theta \cos(2Nt\sin\theta)}{1 - \frac{1}{2}\int_0^\pi \mathrm{d}\theta \cos^2\theta \sin\theta \cos(2Nt\sin\theta) - \frac{1}{2}\int_0^\pi \mathrm{d}\theta \sin^3\theta \cos(2Nt\sin\theta)} - \frac{1}{3}. \tag{5.6}$$

In the limit of $t \to 0$, we obtain

$$b_{11} = b_{22} = -\tfrac{7}{30}, \tag{5.7}$$

$$b_{33} = \tfrac{7}{15}, \tag{5.8}$$

and in the long-time limit ($t \to \infty$) we obtain

$$b_{11} = b_{22} = -\tfrac{1}{6}, \tag{5.9}$$

$$b_{33} = \tfrac{1}{3}. \tag{5.10}$$

These agree well with the DNS results by Gerz & Yamazaki (1993). The small difference at long time can only come from the weak nonlinearity and the effect of the periodic boundary conditions used in DNS.

Figure 5 shows the comparison of the normalized flux with air flow experiments by Yoon & Warhaft (1990). In this case, $Pr = 0.7$, $\overline{Re} = 4050$, $\overline{Fr} = 84.8$. If we set the ratio $PE_0/KE_0 = 0.15$ so that the initial peak value of the normalized flux (0.68) agrees, subsequent time development agrees well. It seems that the excitation of turbulence begins earlier than $t = 0$ in the experiment. The agreement is remarkable considering the likely difference in the initial spectral form of $E(k)$ and $S(k)$. Note the weak countergradient flux ($[-\overline{\rho u_3}/(\overline{\rho^2}^{1/2}\overline{u_3^2}^{1/2})]_{max} \simeq 0.2$) in this case ($Pr < 1$) compared to the previous cases (figures 2 and 3) where $Pr = 1$. The weak countergradient flux for $Pr < 1$ can be inferred from our expression for the flux (4.22) as discussed in §4.

Figure 6 shows the corresponding one-dimensional cospectrum $-k_1\Theta_{\rho 3}(k_1)$. In these figures, positive $-k_1\Theta_{\rho 3}(k_1)$ means countergradient flux. The vertical scale of the RDT results is arbitrary since the modulus of $-\Theta_{\rho 3}(k_1)$ is proportional to the initial energy of the turbulence. We can easily determine the initial energy so that the order of magnitude agrees with the experiments. In spite of the likely difference in the initial energy spectrum forms $E(k)$ and $S(k)$, the time development is qualitatively the same in these figures.

We see that the countergradient flux is retarded at high wavenumber, while it occurs faster at lower wavenumbers. These results for low Prandtl number flow ($Pr < 1$) can be inferred from (4.25). In this case there is a slow development of the countergradient flux at much lower wavenumbers. We should note that the one-dimensional cospectrum (4.25) has a more complicated form than the three-dimensional cospectrum (4.21), so that this development of the countergradient flux at the lowest wavenumbers is not as easily apparent, but can be clarified from (4.25). In fact, the precursor countergradient flux at high wavenumbers occurs even when $Pr = 1$ as we discussed in §4 ! This effect is still apparent at $Pr = 0.7$. Some of these complex differences do not occur in the three-dimensional spectral functions, so that cautious interpretation is necessary of experiments where only one-dimensional spectra are measured.

In figure 6 we observe that the peak wavenumber k_1 in the one-dimensional cospectrum is lower in the experiments than in RDT. This would be partly due to the difference in the initial energy spectrum forms of $E(k)$ and $S(k)$. As noted at the beginning of this section, the spectrum in the usual experiments has an asymptotic form more similar to $E(k), S(k) \propto k^2$ ($k \to 0$), which is different from $E(k), S(k) \propto k^4$ ($k \to 0$) used in the RDT (figure 6*b*). Indeed if we use (5.3) instead of (5.1) and (5.2) in the RDT, the peak wavenumber decreases and approaches the experimental value.

A further comparison with the air flow experiments by Lienhard & Van Atta (1990) (their case of $N = 2.42$ s^{-1} and mesh size $L_0 = 5.08$ cm) is shown in figure 7. In

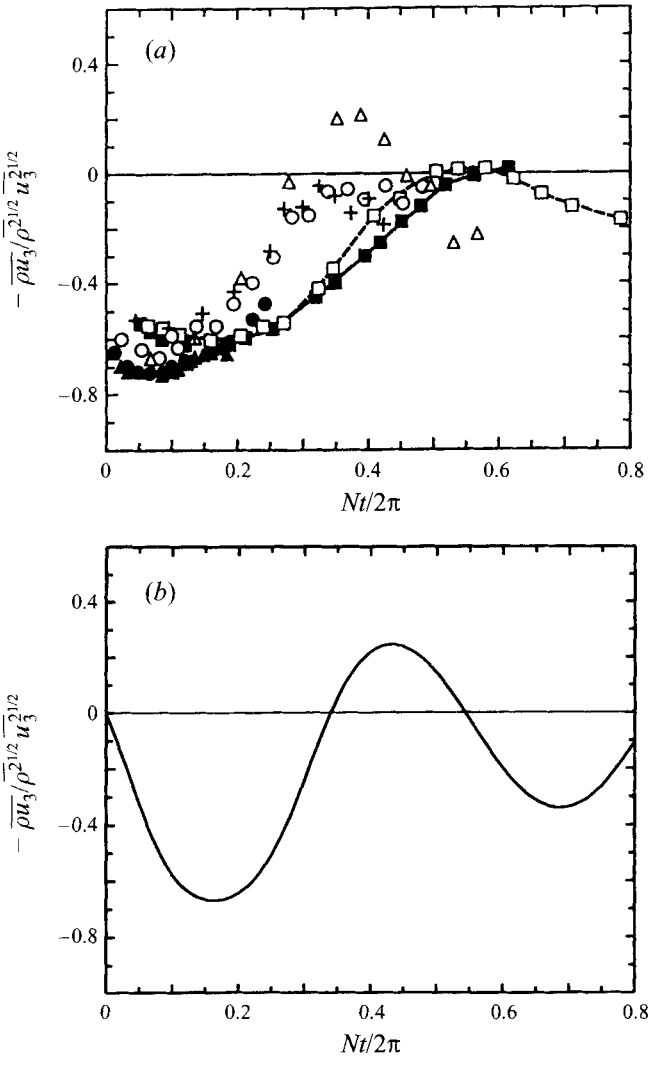

FIGURE 5. Time development of the normalized vertical density flux when $Pr = 0.7$. (*a*) Wind tunnel experiments by Yoon & Warhaft (1990, figure 14*b*, $Fr < 1$ when $Nt/2\pi > 0.15$): △, $\overline{Fr} = 84.8, \overline{Re} = 4050$; ○, $\overline{Fr} = 114, \overline{Re} = 5100$; +, $\overline{Fr} = 127, \overline{Re} = 6070$; •, $\overline{Fr} = 192, \overline{Re} = 6040$; ▲, $\overline{Fr} = 253, \overline{Re} = 5670$. Wind tunnel experiments by Lienhard & Van Atta (1990, figure 2*b*, $Fr < 1$ when $Nt/2\pi > 0.25$); □, $\overline{Fr} = 17.1, \overline{Re} = 7100$; ■, $\overline{Fr} = 22, \overline{Re} = 7900$. (*b*) RDT ($\overline{Fr} = 84.8, \overline{Re} = 4050$, $PE_0/KE_0 = 0.15$, $k_0 = 30$).

this case $Pr = 0.7$, $\overline{Re} = 7100$, $\overline{Fr} = 17.1$ and $PE_0/KE_0 = 0.14$. Here, PE_0/KE_0 is estimated from its value at their most upstream measuring point. In their experiments, countergradient flux, if it occur is very weak. Very weak (or vanishing) countergradient flux at $Pr = 0.7$ cannot be explained by RDT, although the reduction of Pr from 1 leads to larger cogradient flux and weaker countergradient flux as we can infer from (4.25). A countergradient flux localized at low wavenumbers (see their figure 20) requires an explanation based on the nonlinearity of turbulence. As discussed in §2, the validity of RDT is high when the turbulent Froude number Fr is small. As shown in figure 18 of Yoon & Warhaft (1990), Fr is smaller (about 1/2) in the experiment

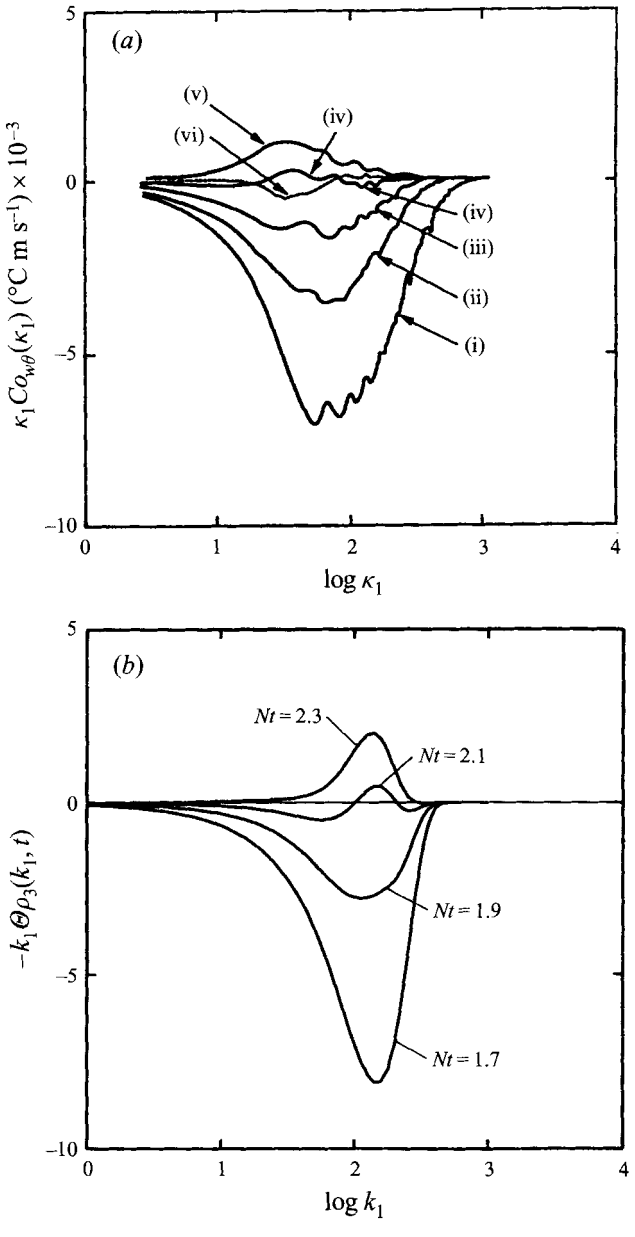

FIGURE 6. Time development of the one-dimensional spectrum $-k_1\Theta_{\rho 3}(k_1, t)$ corresponding to figure 5 ($Pr = 0.7$, $\overline{Fr} = 84.8$, $\overline{Re} = 4050$). (*a*) Wind tunnel experiments by Yoon & Warhaft (1990, figure 15*b*, x:distance from the grid, M:mesh length of the grid, $Fr < 1$ where $x/M > 76.5$.) (i) $x/M = 36.5$; (ii) 76.5; (iii) 116.5; (iv) 156.5; (v) 196.5; (vi) 236.5. (*b*) RDT ($PE_0/KE_0 = 0.15$, $k_0 = 30$).

of Yoon & Warhaft (1990) than in the experiment by Lienhard & Van Atta (1990) at least for the initial stage $0 < Nt/2\pi < 0.4$. Thus the nonlinear effect is smaller in the experiment of Yoon & Warhaft (1990). This explains why the experiments by Yoon & Warhaft (1990) give better agreement with RDT. In figure 5(*a*), $Fr < 1$ where $Nt/2\pi > 0.15$ (Yoon & Warhaft 1990, figure 18), while in figure 7(*a*), $Fr < 1$

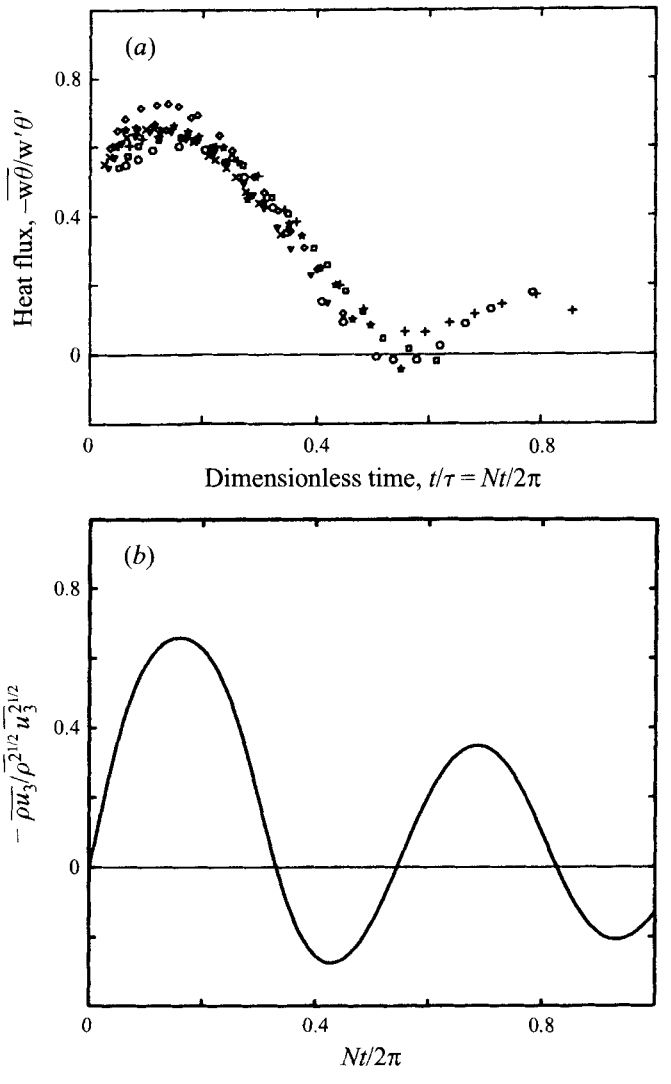

FIGURE 7. Time development of the normalized vertical density flux when $Pr = 0.7$. (*a*) Wind tunnel experiments by Lienhard & Van Atta (1990, figure 2*b*, $Fr < 1$ when $Nt/2\pi > 0.25$): ○, $\overline{Fr} = 17.1, \overline{Re} = 7100$; □, $\overline{Fr} = 22, \overline{Re} = 7900$; ▽, $\overline{Fr} = 33, \overline{Re} = 8400$; ×, $\overline{Fr} = 42, \overline{Re} = 8400$; +, $\overline{Fr} \approx 31, \overline{Re} \approx 3400$; ⋆, $\overline{Fr} = 47, \overline{Re} = 4400$; ◇, $\overline{Fr} \approx 62, \overline{Re} \approx 4200$. (*b*) RDT ($\overline{Fr} = 17.1$, $\overline{Re} = 7100$, $PE_0/KE_0 = 0.14$, $k_0 = 30$).

only where $Nt/2\pi > 0.25$. Yoon & Warhaft also considered the difference in the ratio of the initial temperature fluctuations to the mean flow energy as one of the possible explanations for the different strength of the countergradient flux in the two experiments. In their most stable cases, the ratio in the experiments by Lienhard & Van Atta was about five times larger than that in Yoon & Warhaft. According to Yoon & Warhaft(1990), Dr M. Rogers found in his DNS that if his code is run with substantial initial temperature fuctuations, no counter heat flux occurs. Therefore, their surmise is consistent with our explanation.

If we consider the modelling of turbulence, we should use a lower effective Prandtl number so that the countergradient flux becomes weaker. At the same time, we have

to use a smaller Reynolds number so that the cogradient flux does not become too large.

It is of interest here to note the time development of $\overline{u_1^2}(t)$ and $\overline{u_3^2}(t)$. In the experiments by Lienhard & Van Atta (1990, figures 5, 6) and Yoon & Warhaft (1990, figure 4), they note that $\overline{u_1^2}(t)$ shows similar decay to isotropic unstratified turbulence, almost independent of the Froude number $\overline{Fr}$. On the other hand, $\overline{u_3^2}(t)$ shows deviations from the isotropic value at long time, which are larger for stronger stratification (smaller $\overline{Fr}$). These results can be qualitatively explained by (4.24) or (4.29) of our theory. First consider $\overline{u_3^2}(t)$ given by (4.24). When time t is small, the contributions from the term

$$E(k)\left[\tfrac{1}{2}(\nu-\kappa)^2k^4\cos\alpha t+\tfrac{1}{2}(\nu-\kappa)k^2\alpha\sin\alpha t\right] \tag{5.11}$$

are large especially at high wavenumber since this term contains k^4 and k^2. This term represents essentially a no-stratification (isotropic turbulence) effect and exists even when $N=\kappa=0$, showing simple exponential decay of $E(k)$ with time. Note here that this term does not oscillate with time at large k, since α becomes pure imaginary. However, the effect of this term decays rapidly because the high-wavenumber components decay faster with time owing to the viscosity and the diffusion. The examination of the contribution of the two terms in (4.24) in the long-time limit ($t\to\infty$) shows that the effect of the first term of (5.11) decays like $t^{-(l+3)}$ and the second term of (5.11) decays like $t^{-(l+2)}$ if the initial spectra are given by (4.40) and (4.41). Where α is imaginary, (5.11) is the 'Pearson & Linden' mode discussed in §4.2 but it decays faster like $t^{-(l+9/2)}$. Then, as time goes on, the effect of the lower-wavenumber components becomes dominant. At this stage, the effect of the term

$$N^2\sin^2\theta\left[(E(k)+2S(k))+(E(k)-2S(k))\cos\alpha t\right] \tag{5.12}$$

becomes dominant. At low wavenumbers with real α, this term shows oscillatory behaviour with time, leading to the oscillation of $\overline{u_3^2}(t)$ particularly when N is large. The experimental results reported by Yoon & Warhaft (1990, figure 4) show the time oscillation of $\overline{u_3^2}(t)$ at their lowest Froude number $\overline{Fr}$ (at largest N). Their measurement of the time development of Θ_{33} (their figure 5) shows that only the low-wavenumber components oscillate with time, while the high-wavenumber components show monotonic decay. This is again consistent with our results. When the time t becomes much larger ($t\to\infty$), only the first term of (5.12), i.e. $N^2\sin^2\theta(E(k)+2S(k))$, becomes effective and (4.24) reduces to (4.50). Then the oscillations must cease in the long time. Examination of the contribution of (5.12) in the integral representation of $\overline{u_3^2}(t)$ shows that in the long-time limit, the first term of (5.12) decays like $t^{-(l+1/2)}$ while the second term decays like $t^{-(l+1)}$. This is consistent with our qualitative discussions above.

We should note at the same time that the previous experimental data for $\overline{u_1^2}(t)$ and $\overline{u_3^2}(t)$ are usually plotted as functions of the distance from the grid x/M, i.e. of t, and not of Nt. Since the oscillatory behaviour in (4.24) is mainly regulated by Nt, a larger time t is necessary to identify the oscillation if N is small. This is exactly true when $Pr=1$ (see (4.30)). Even when $Pr\neq 1$, in which case the integral of the complicated function of αt (see (4.24)) determine the time development, the main contribution as time elapses comes from near $k=0$ and $\theta=\pi/2$, which makes $\alpha=2N$. This might be another reason why in the previous experiments the oscillation in $\overline{u_3^2}(t)$ was not observed when N is small.

Next we consider $\overline{u_1^2}(t)$. Since the expression for $\overline{u_1^2}(t)$ for general Pr is lengthy, we have not given the results in §4. However, we can predict the qualitative behaviour from the results for $Pr = 1$ given by (4.29). As we have seen in the inviscid results (§3), the integral

$$\int_0^\pi \mathrm{d}\theta \cos^2\theta \sin\theta \cos(2Nt\sin\theta) \tag{5.13}$$

in (4.29) becomes zero if we apply the steepest descents. This shows that this integral decays faster than $\propto t^{-1/2}$. We could see this effect also in the difference between figures 1(*a*) and 1(*b*), where the results were for inviscid fluid. Since the integral (5.13) is the only part in the expression for $\overline{u_1^2}(t)$ that contains N, the effect of stratification decays very rapidly in $\overline{u_1^2}(t)$ compared to $\overline{u_3^2}(t)$. This explains why in the experiments, the effect of N (or $\overline{Fr}$), in particular the oscillatory behaviour with time, was not observed in the time development of $\overline{u_1^2}(t)$. As we have seen in figure 4, for the time development of the anisotropy tensor b_1, b_2 and b_3 there is quantitative agreement between DNS and RDT when the initial turbulence energy is small. This indeed shows that if the nonlinear effect is weak, RDT predicts quantitatively the time development of $\overline{u_1^2}(t)$ and $\overline{u_3^2}(t)$.

From the results of a DNS similar to Métais & Herring (1989), Kimura & Herring (1996) calculated the velocity gradient skewness factors $S_x = -\overline{(\partial u/\partial x)^3}/\overline{(\partial u/\partial x)^2}^{3/2}$ and $S_z = -\overline{(\partial w/\partial z)^3}/\overline{(\partial w/\partial z)^2}^{3/2}$ and showed that S_z reduces to nearly zero more rapidly with time than S_x. This suggests that the nonlinear energy transfer in the horizontal direction, which would be indicated by S_x, is less easily suppressed by the stratification and this would also explain why $\overline{u_1^2}(t)$, compared to $\overline{u_3^2}(t)$, shows a decay rate more similar to isotropic neutral turbulence ($Fr = \infty$), in which nonlinear effects are larger.

Figure 8 shows the comparison with the thermally stratified water experiments by Komori & Nagata (1995). Their experiments are for two-layer flow and not for a continously stratified flow, but their one-dimensional cospectrum shows clearly the effect of the large Prandtl number ($Pr > 1$). Here, $Pr = 6$, $\overline{Re} = 2500$, $\overline{Fr} = 2.86$ (at the interface of the two fluids) and the value of PE_0/KE_0 estimated from the initial maximum of their normalized vertial density flux ($\simeq 0.6$) is 0.11. The comparison with RDT results shows good agreement in that the enhanced countergradient flux at high wavenumbers exists. In the salt-water experiments by Itsweire *et al.* (1986) no countergradient flux was observed at high wavenumber, but Lienhard & Van Atta (1990) speculate that this might have been the result of relatively poor high-wavenumber resolution in their experiments. We should be careful about the interpretation of the one-dimensional spectrum since, as already noted in §4, a transitory countergradient flux at high wavenumbers appears even when $Pr = 1$. However, comparison of the results of Komori & Nagata with the corresponding low Prandtl number ($Pr = 0.7$) wind tunnel experiments for two-layer flow by Jayesh & Warhaft (1994) show clear differences. As in the continuously stratified fluid, Jayesh & Warhaft found that countergradient flux first appears at low wavenumbers. We should mention here that in figure 8(*a*), the turbulent Froude number Fr was less than 1 where $x/M > 10$ (Personal communication with Komori & Nagata), showing the validity of the linear theory there.

To understand the decay of turbulence due to viscosity and diffusion, we show in figure 9 the time development of the turbulence energy from the DNS of Gerz & Yamazaki (1993) (their case C, i.e. the case with the smallest turbulence energy)

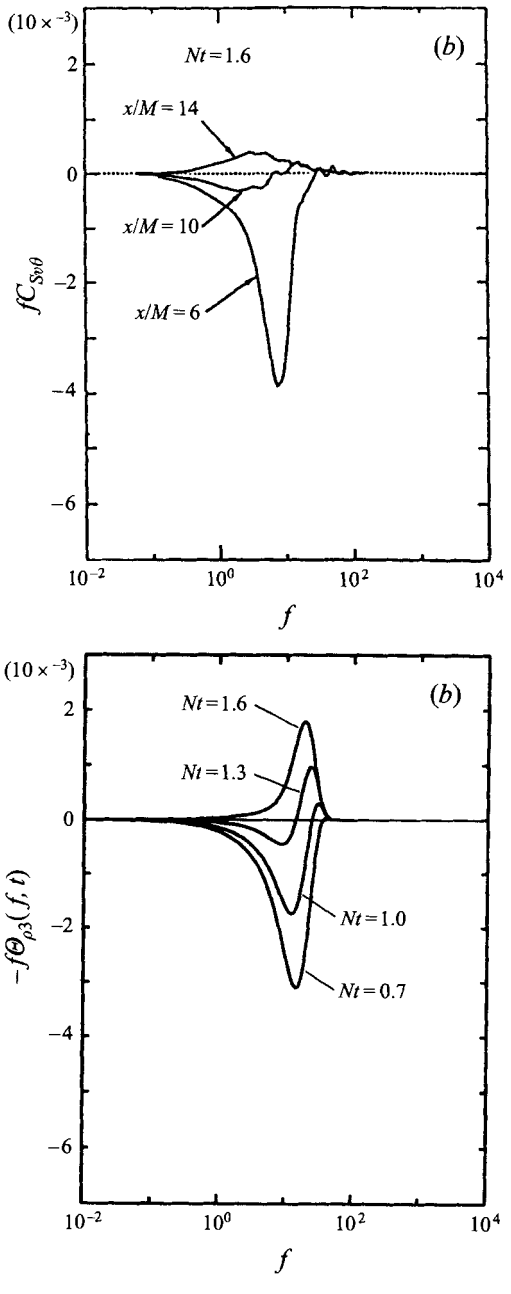

FIGURE 8. Time development of the one-dimensional spectrum $-f\Theta_{\rho 3}(f,t)$ ($f = k_1 U/2\pi$) near the time when $\overline{\rho u_3}$ first vanishes ($Pr = 6$, $\overline{Re} = 2500$, $\overline{Fr} = 2.86$). (*a*) Water-tank experiments by Komori & Nagata (1995, figure 9*b*, x: distance from the grid, M: mesh length of the grid, $Fr < 1$ holds where $x/M > 10$). (*b*) RDT ($PE_0/KE_0 = 0.11$, $k_0 = 25$).

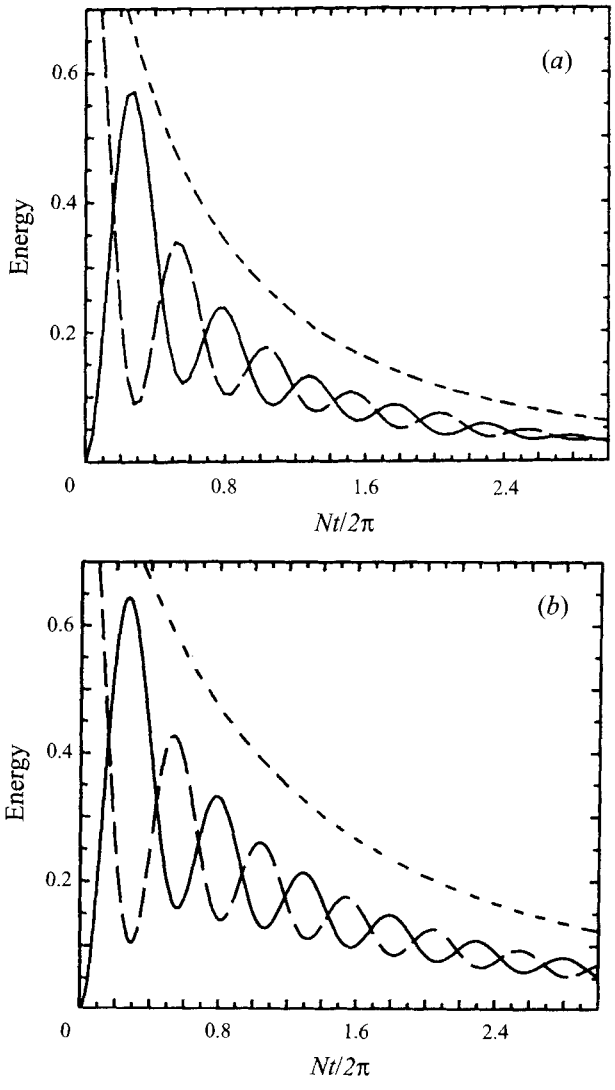

FIGURE 9. Time development of the kinetic, potential and total turbulence energy when $Pr = 1$ and $KE_0 = 0$. ————, KE/KE_0; — — — —, PE/PE_0; - - - - - -, TE/TE_0. (*a*) DNS by Gerz & Yamazaki (1993, figure 1*c*). (*b*) RDT.

and the corresponding results from RDT. In this case $Pr = 1$, $E(k) = 0$ and $S(k)$ has the form of (5.2). RDT the turbulent kinetic energy $KE(t)$ and the turbulent potential energy $PE(t)$ can be easily calculated from (4.28)–(4.30) by setting $E(k) = 0$. Then, the total turbulence energy is obtained as $TE(t) = KE(t) + PE(t)$. The results are

$$KE(t) = \tfrac{1}{2}(\overline{u_1^2} + \overline{u_2^2} + \overline{u_3^2})$$

$$= \frac{1}{2}\int_0^\infty \mathrm{d}k S(k)\mathrm{e}^{-2\nu k^2 t}\left[1 - \frac{1}{2}\int_0^\pi \mathrm{d}\theta \sin\theta \cos(2Nt\sin\theta)\right], \qquad (5.14)$$

$$PE(t) = \frac{1}{2N^2}\overline{\rho^2}$$
$$= \frac{1}{2}\int_0^\infty \mathrm{d}kS(k)\mathrm{e}^{-2\nu k^2 t}\left[1 + \frac{1}{2}\int_0^\pi \mathrm{d}\theta \sin\theta \cos(2Nt\sin\theta)\right], \tag{5.15}$$

and

$$TE(t) = \int_0^\infty \mathrm{d}kS(k)\mathrm{e}^{-2\nu k^2 t}. \tag{5.16}$$

We can calculate this integral analytically by substituting (5.2) and find the decay ratio to be

$$\frac{TE(t)}{TE(0)} = \frac{\int_0^\infty \mathrm{d}kS(k)\mathrm{e}^{-2\nu k^2 t}}{\int_0^\infty \mathrm{d}kS(k)} = \left(\frac{1}{1+\nu k_0^2 t}\right)^{5/2}. \tag{5.17}$$

Using the same Reynolds number $Re = 57.4$ and the same peak wavenumber in the initial energy spectrum $k_0 = (8\pi)^{1/2}$ as in Gerz & Yamazaki (1993), we obtain the RDT counterpart (figure 9*b*) of the DNS results (figure 9*a*). The comparison is good except that there is a slightly faster decay in DNS. Thus the effective viscosity/diffusion (in this case $\nu = \kappa$) is a little larger in DNS. If the numerical viscosity is negligible in DNS, the difference comes only from the nonlinearity. This supports again the conjecture that, to incorporate nonlinearity effects, use of lower Prandtl and Reynolds numbers are appropriate. When the nonlinearity is not large, its effect would be well described by such choices. As we have seen in figures 2 and 4, the non-dimensional ratio of the covariances agrees excellently with RDT, even when there are some deviations in the decay rate of each covariances or the turbulent energies (figure 9). This shows that the functional forms of the covariances are not affected by the nonlinearity, the only differences being in the effective value of the viscosity/diffusion coefficient or the Reynolds/Prandtl numbers.

It is of interest that, in the long-time limit ($Nt \to \infty$), RDT shows a decay proportional to $t^{-5/2}$. This is exactly the same as the 'final' stage of decay of three-dimensional unstratified turbulence (Batchelor 1953) having the same low-wavenumber spectrum $\propto k^4$. This rate is greater than that of the initial, self-similar and inertially dominated stage for which $KE(t) \propto t^{-r}$, where $1 \leqslant r < 1.3$. The decay rate in the long-time limit depends on the form of $S(k)$ near $k = 0$ so that if $S(k) \propto k^2$ then the result differs from (5.17) and becomes $TE(t) \propto t^{-3/2}$, as we have seen in §4. Gerz & Yamazaki (1993) did not give results for a very long-time development. In the most energetic case B of Gerz & Yamazaki (see their figure 2), which shows a tendency to isotropy in a rather short time, the decay is proportional to $t^{-1.3}$ when $Nt/2\pi > 1.0$, while the smallest turbulence energy case C showed much slower decay at least for $Nt/2\pi < 3$. In comparison of the simplified two-point closure EDQNM model and its linearized version (RDT) with the DNS results, van Haren, Staquet & Cambon (1996) found that the decay rate in RDT is smaller than EDQNM and DNS when $Nt/2\pi \leqslant 1$. These results can be attributable to the weaker or no nonlinear transfer of energy in strongly stratified turbulence or in RDT to smaller scales where the energy is mainly dissipated. However, the decay rate in stratified turbulence changes with the elapsed time. Indeed, the long-time simulation of Métais & Herring (1989) shows an 'increasing' decay rate with time similar to (5.17). (See run 2A of their figure 13, where $Pr = 1$, $E(k)$ is given by (5.1), and $S(k) = 0$. This difference in the initial energy spectra $E(k)$ and $S(k)$ does not change the theoretical prediction

of total energy decay given by (5.17).) In (5.17) the decay rate increases from t^0 at $t = 0$ to $t^{-5/2}$ as $t \to \infty$. In their final period of computation ($Nt = 100\pi$), the energy decays like t^{-2}, which is tending to the RDT result. Finally it is important to note that (5.17) explicitly shows that the decay rate is independent of the stratification parameter N and is determined by the viscosity ν, as was suggested by van Haren *et al.* (1996) from their numerical results. Therefore care should be taken if time is non-dimensionalized by N in discussions of the decay rate.

6. Conclusions

We have investigated the time development of stratified unsheared turbulence using rapid distortion theory (RDT). The result shows that the time-dependent oscillations, including the countergradient phenomena, can largely be explained in terms of phase lags in linear oscillations rather than in terms of any new kind of nonlinear mixing processes. Our main results can be summarized as follows.

For inviscid fluid, we have obtained the time-dependent covariances in explicit analytical forms and showed their short- and long-time limits. These limits have clarified that the initial turbulent kinetic and potential energy determine the final partition of energy among each velocity component and density perturbation. The covariances depend only on the initial total kinetic and potential energy and not on the precise form of the energy spectra. The oscillation period of the covariances, including the zeros of the vertical density flux, are completely independent of the initial condition.

For viscous/diffusive fluids, we have given the analytical form of the time-dependent three-dimensional spectral functions and expressed the corresponding one-dimensional spectra and covariances by rather simple integrals, which enable us to see the effect of the Prandtl and Reynolds numbers clearly. We have found that a high Prandtl number ($Pr > 1$) leads to the countergradient flux occurring at high wavenumber, while a low Prandtl number ($Pr < 1$) inhibits the countergradient flux at high wavenumber. These explain the difference between the water tank and wind tunnel experiments. The analysis shows that special care is needed in interpreting the three-dimensional and the one-dimensional spectra. One-dimensional spectra show the transitory countergradient flux at high wavenumber even when $Pr = 1$, which does not occur in the corresponding three-dimensional spectra.

For viscous/diffusive fluids, the asymptotic forms of the variances and covariances in the long-time limit are determined by the initial spectral form of the kinetic and potential energy, i.e. $E(k)$ and $S(k)$, near $k = 0$. Specifically, it has been shown that the ratio of the turbulent potential energy to vertical kinetic energy in the long-time limit is 3/2 and independent of any initial conditions (other than the assumption of isotropy), Prandtl number, Reynolds number and Froude number. This should help modelling real atmospheric or oceanic turbulence (Schumann & Gerz 1995). The asymptotic form of the normalized vertical density flux $\overline{\rho u_3}/(\overline{\rho^2}^{1/2}\overline{u_3^2}^{1/2})$ also shows similar independence of the initial conditions and the non-dimensional parameters.

When $Pr = 1$, all the wavenumber components in the three-dimensional spectrum function oscillate in phase, as in an inviscid fluid. Then the effects of viscosity and diffusion are limited to the damping of all the wavenumber components in phase. The oscillation periods of the covariances also agree with those for an inviscid fluid and do not depend on the initial conditions (except for the assumption of isotropy). If $Pr = 1$ and the initial turbulent kinetic or potential energy spectrum has the

same form except for the multiplying constant, the non-dimensional ratios of the covariances, such as the normalized vertical density flux or the anisotropy tensor, agree exactly with the inviscid results.

To estimate certain effects of nonlinearity which might dominate in high Reynolds number turbulence (cf. Townsend 1976), the use of an effective (eddy) viscosity and diffusion coefficient has been considered. (There are of course other effects of nonlinearity, such as modulating the frequency of the oscillation, not described by this approximation.) This leads the eddy Prandtl number Pr_t (see Townsend 1976, p. 358) and Reynolds number to be smaller than the molecular values. Applying these values in the linear theory leads to the strength of the countergradient flux decreasing and our results become closer to the moderate Reynolds number laboratory experiments. We note that in atmospheric measurements of unsteady stably stratified turbulence at very high Reynolds number (where $Re \approx 10^4$ and $Fr \simeq 1$) such as those described by Nai-ping, Neff & Kaimal (1983), countergradient fluxes were observed. Significant countergradient fluxes also occur when density layers emerge in decaying turbulence. Barenblatt *et al.* (1993) proposed a novel mechanism based on a nonlinear time-delay model of Richardson number-dependent eddy diffusion. The range of applicability of this concept needs further examinations.

Finally we note that in steady or slowly varying stably stratified turbulence at high Reynolds numbers, such as described by Hunt *et al.* (1985), no systematic countergradient fluxes were observed.

REFERENCES

Barenblatt, G. I., Bertsch, M., Dal Passo, R., Prostokishin, V. M. & Ughi, M. 1993 A mathematical model of turbulent heat and mass transfer in stably stratified shear flow. *J. Fluid Mech.* **253**, 341–358.

Batchelor, G. K. 1953 *The Theory of Homogeneous Turbulence.* Cambridge University Press.

Batchelor, G. K. & Proudman, I. 1956 The large-scale structure of homogeneous turbulence. *Phil. Trans. R. Soc. Lond.* A **248**, 369–405.

Britter, R. E., Hunt, J. C. R., Marsh, G. L. & Snyder, W. H. 1983 The effect of stable stratification on turbulent diffusion and the decay of grid turbulence. *J. Fluid Mech.* **127**, 27–44.

Deissler, R. G. 1962 Turbulence in the presence of a vertical body force and temperature gradient. *J. Geophys. Res.* **67**, 3049–3062.

Derbyshire, S. H. & Hunt, J. C. R. 1985 Structure of turbulence in stably stratified atmospheric boundary layers; Comparison of large eddy simulations and theoretical results. In *Waves and Turbulence in Stably Stratified Flows* (ed. S. D. Mobbs & J. C. King), pp. 23–59. Clarendon.

Gerz, T. & Yamazaki, H. 1993 Direct numerical simulation of buoyancy-driven turbulence in stably stratified fluid. *J. Fluid Mech.* **249**, 415–440.

Haren, L. van, Staquet, C. & Cambon, C. 1996 Decaying stratified turbulence: comparison between a two-point closure EDQNM model and direct numerical simulations. *Dyn. Atmos. Oceans* **23**, 217–233.

Hinch, E. J. 1991 *Perturbation Methods.* Cambridge University Press.

Hunt, J. C. R. & Carruthers, D. J. 1990 Rapid distortion theory and the 'problems' of turbulence. *J. Fluid Mech.* **212**, 497–532.

Hunt, J. C. R., Kaimal, J. C. & Gaynor, J. E. 1985 Some observations of turbulence structure in stable layers. *Q. J. R. Met. Soc.* **111**, 793–815.

Hunt, J. C. R., Stretch, D. D. & Britter, R. E. 1988 Length scales in stably stratified turbulent flows and their use in turbulence models. In *Stably Stratified Flow and Dense Gas Dispersion* (ed. J. S. Puttock), pp. 285–321. Clarendon.

Hunt, J. C. R. & Vassilicos, J. C. 1991 Kolmogorov's contributions to the physical and geometrical understanding of small-scale turbulence and recent developments. *Proc. R. Soc. Lond.* A **434**, 183–210.

ITSWEIRE, E. C., HELLAND, K. N. & VAN ATTA, C. W. 1986 The evolution of grid-generated turbulence in a stably stratified fluid. *J. Fluid Mech.* **162**, 299–338.

JAYESH & WARHAFT, Z. 1994 Turbulent penetration of a thermally stratified interfacial layer in a wind tunnel. *J. Fluid Mech.* **277**, 23–54.

KIMURA, Y. & HERRING, J. R. 1996 Diffusion in stably stratified turbulence. submitted to *J. Fluid Mech.*

KOMORI, S. & NAGATA, K. 1995 Effects of molecular diffusivities on counter-gradient scalar and momentum transfer in strong stable stratification. submitted to *J. Fluid Mech.*

KOMORI, S., UEDA, H., OGINO, F. & MIZUSHINA, T. 1983 Turbulence structure in stably stratified open-channel flow. *J. Fluid Mech.* **130**, 13–26.

LIENHARD, J. H. & VAN ATTA, C. W. 1990 The decay of turbulence in thermally stratified flow. *J. Fluid Mech.* **210**, 57–112.

LINDEN, P. F. 1980 Mixing across density interfaces produced by grid turbulence. *J. Fluid Mech.* **100**, 691–709.

MÉTAIS, O. & HERRING, J. 1989 Numerical simulations of freely evolving turbulence in stably stratified fluids. *J. Fluid Mech.* **202**, 117–148.

NAI-PING, L., NEFF, W. D. & KAIMAL, J. C. 1983 Wave and turbulence structure in a disturbed nocturnal inversion. In *Studies of Nocturnal Stable Layers at BAO* (ed. J. C. Kaimal), pp. 53–73. NOAA.

NIEUWSTADT, F. T. M. 1984 The turbulent structure of the stable, nocturnal boundary layer. *J. Atmos. Sci.* **41**, 2202–2216.

PEARSON, H. J. & LINDEN, P. F. 1983 The final stage of decay of turbulence in stably stratified fluid. *J. Fluid Mech.* **134**, 195–203.

PEARSON, H. J., PUTTOCK, J. S. & HUNT, J. C. R. 1983 A statistical model of fluid-element motions and vertical diffusion in a homogeneous stratified turbulent flow. *J. Fluid Mech.* **129**, 219–249.

RILEY, J. J., METCALFE, R. W. & WEISSMAN, M. A. 1981 Direct numerical simulations of homogeneous turbulence in density stratified fluids. In *Nonlinear Properties of Internal Waves.* AIP Conference Proc. vol. 76, pp. 79–112. American Institute of Physics.

SAFFMAN, P. G. 1967 The large-scale structure of homogeneous turbulence. *J. Fluid Mech.* **27**, 581–593.

SCHUMANN, U. & GERZ, T. 1995 Turbulent mixing in stably stratified shear flows. *J. Appl. Met.* **34**, 33–48.

THORODDSEN, S. T. & VAN ATTA, C. W. 1995 The effects of vertical contraction on turbulence dynamics in a stably stratified fluid. *J. Fluid Mech.* **285**, 371–406.

TOWNSEND, A. A. 1976 *The Structure of Turbulent Shear Flow.* Cambridge University Press.

YOON, K. & WARHAFT, Z. 1990 The evolution of grid generated turbulence under conditions of stable thermal stratification. *J. Fluid Mech.* **215**, 601–638.